Available online at www.sciencedirect.com

ScienceDirect

Geochimica et Cosmochimica Acta 228 (2018) 95–118

Geochimica et Cosmochimica Acta

www.elsevier.com/locate/gca

Geochemistry of fluids from Earth's deepest ridge-crest hot-springs: Piccard hydrothermal field, Mid-Cayman Rise

Jill M. McDermott [a,*], Sean P. Sylva [a], Shuhei Ono [b], Christopher R. German [a], Jeffrey S. Seewald [a]

[a] *Woods Hole Oceanographic Institution, Woods Hole, MA 02543, USA*

[b] *Massachusetts Institute of Technology, Department of Earth, Atmospheric and Planetary Sciences, Cambridge, MA 02139, USA*

Received 26 May 2017; accepted in revised form 15 January 2018; available online 13 February 2018

Abstract

Hosted in basaltic substrate on the ultra-slow spreading Mid-Cayman Rise, the Piccard hydrothermal field is the deepest currently known seafloor hot-spring (4957–4987 m). Due to its great depth, the Piccard site is an excellent natural system for investigating the influence of extreme pressure on the formation of submarine vent fluids. To investigate the role of rock composition and deep circulation conditions on fluid chemistry, the abundance and isotopic composition of organic, inorganic, and dissolved volatile species in high temperature vent fluids at Piccard were examined in samples collected in 2012 and 2013.

Fluids from the Beebe Vents and Beebe Woods black smokers vent at a maximum temperature of 398 °C at the seafloor, however several lines of evidence derived from inorganic chemistry (Cl, SiO_2, Ca, Br, Fe, Cu, Mn) support fluid formation at much higher temperatures in the subsurface. These high temperatures, potentially in excess of 500 °C, are attainable due to the great depth of the system. Our data indicate that a single deep-rooted source fluid feeds high temperature vents across the entire Piccard field. High temperature Piccard fluid H_2 abundances (19.9 mM) are even higher than those observed in many ultramafic-influenced systems, such as the Rainbow (16 mM) and the Von Damm hydrothermal fields (18.2 mM). In the case of Piccard, however, these extremely high H_2 abundances can be generated from fluid-basalt reaction occurring at very high temperatures.

Magmatic and thermogenic sources of carbon in the high temperature black smoker vents are described. Dissolved ΣCO_2 is likely of magmatic origin, CH_4 may originate from a combination of thermogenic sources and leaching of abiotic CH_4 from mineral-hosted fluid inclusions, and CO abundances are at equilibrium with the water–gas shift reaction. Longer-chained n-alkanes (C_2H_6, C_3H_8, n-C_4H_{10}, i-C_4H_{10}) may derive from thermal alteration of dissolved and particulate organic carbon sourced from the original seawater source, entrainment of microbial ecosystems peripheral to high temperature venting, and/or abiotic mantle sources. Dissolved ΣHCOOH in the Beebe Woods fluid is consistent with thermodynamic equilibrium for abiotic production via ΣCO_2 reduction with H_2 at 354 °C measured temperature. A lack of ΣHCOOH in the relatively higher temperature 398 °C Beebe Vent fluids demonstrates the temperature sensitivity of this equilibrium.

Abundant basaltic seafloor outcrops and the axial location of the vent field, along with multiple lines of geochemical evidence, support extremely high temperature fluid-rock reaction with mafic substrate as the dominant control on Piccard fluid chemistry. These results expand the known diversity of vent fluid composition, with implications for supporting microbiological life in both the modern and ancient ocean.

* Corresponding author at: Department of Earth and Environmental Sciences, Lehigh University, Bethlehem, PA 18015, USA.
E-mail address: jillmmcdermott@alum.mit.edu (J.M. McDermott).

https://doi.org/10.1016/j.gca.2018.01.021
0016-7037/

1. INTRODUCTION

Located in the basaltic neovolcanic zone at 4957–4987 m depth on the Mid-Cayman Rise, the Piccard vent field is Earth's deepest known mid-ocean ridge hydrothermal system (Beaulieu et al., 2013). The chemical diversity expressed in fluids venting from axial hot-springs is reflective of a broad spectrum of physical, chemical, and biological processes that transform the seawater source fluid during convective circulation through the oceanic crust (Von Damm, 1995; Alt, 1995; Von Damm and Lilley, 2004; Butterfield et al., 2004). Due to its extreme depth, the Piccard hydrothermal system represents an excellent opportunity to extend our understanding of the effects of pressure on deep-sea vent fluid geochemistry. In many hydrothermal systems, pressure plays a fundamental role in regulating temperatures because maximum fluid temperatures are influenced by pressure-dependent physical properties such as buoyancy and may ultimately be limited by the two-phase boundary of seawater. For example, the hottest vent fluids previously measured at the seafloor at the basalt-hosted Turtle Pits field on the Southern Mid-Atlantic Ridge were actively phase separating at 407 °C and 2990 m depth, conditions consistent with the two-phase boundary of seawater (Koschinsky et al., 2008). Due to the much greater axial depth at Piccard, the two-phase boundary at the seafloor occurs at 483 °C (Bischoff and Rosenbauer, 1988) creating the potential for circulating fluids to attain substantially higher temperatures in the oceanic lithosphere relative to hydrothermal fluids from shallower portions of the global mid-ocean ridge system.

The possibility that temperatures in hydrothermal reaction zones at the Mid-Cayman Rise approach or exceed 483 °C has profound implications for the composition of hot-spring fluids venting at the seafloor. Due to the strong dependence of the thermodynamic properties of aqueous fluids and minerals on temperature and pressure, thermodynamic models of fluid-rock interaction in the oceanic lithosphere predict large variations in fluid composition with increasing temperature, especially at and above the critical point of seawater (Bowers et al., 1985; Seyfried et al., 1991; McCollom and Shock, 1998). Much of this variation can be attributed to changes in the solvent properties of H_2O (Brimhall and Crerar, 1987; Oelkers and Helgeson, 1990; Helgeson, 1992) that greatly affect the stability of aqueous complexes. Moreover, the impact of phase separation on vent fluid chemistry is highly dependent on the temperature and pressure conditions during phase separation due to equilibrium partitioning of aqueous species between vapor and brine phases (Berndt and Seyfried, 1997; Berndt and Seyfried, 1990; Foustoukos and Seyfried, 2007a).

Presented here is a chemical and isotopic characterization of hydrothermal fluids collected in 2012 and 2013 at the Piccard hydrothermal field that can be used to examine the effects of high pressure and temperature on water-rock reaction. The origins of dissolved inorganic, organic and volatile species in the high temperature $\leq$398 °C mafic-hosted 'black smoker' Piccard vents are examined. The origins of organic compounds are evaluated, including consideration of a combination of thermogenesis of particulate and dissolved organic carbon inputs and abiotic mantle-derived hydrocarbons. In addition, the abiotic generation of aqueous formate species ($\Sigma HCOOH = HCOOH + HCOO^-$) is investigated.

2. GEOLOGIC SETTING AND SITE DESCRIPTION

The Mid-Cayman Rise is an ultra-slow spreading ridge (15–17 mm/yr full rate) (Rosencrantz et al., 1988) located in the Cayman Trough that is bounded by the North American plate to the north, the Caribbean plate to the south, and the Gonave microplate to the east. Despite the proximity of continental and arc crust (Perfit and Heezen, 1978; Pindell and Barrett, 1990), there is no evidence for a subducted slab component in Cayman Trough basalts (Hayman et al., 2011). Mid-ocean ridge basalts from the Mid-Cayman Rise are compositionally fairly homogenous and consist of a moderately evolved basaltic endmember generated from low melt extent in a relatively cold mantle (Elthon et al., 1995; Klein and Langmuir, 1987).

The Piccard hydrothermal field is located on the eastern flank of a 12 km long volcanic ridge that runs from 18°27′N to 18°34′N through the axial trough of the Mid-Cayman Rise (Kinsey and German, 2013) (Fig. 1a). The site was discovered in 2009–2010 through a combination of plume surveys conducted using the hybrid remotely operated vehicle (HROV) *Nereus* in autonomous mode and a conductivity, temperature, depth instrument (CTD) (German et al., 2010) followed by further surveys with the autonomous underwater vehicle *AUTOSUB* and the wireline vehicle *HYBIS* (Connelly et al., 2012). Detailed mapping of the site was conducted by the remotely operated vehicle (ROV) *Jason II* in 2012 (Kinsey and German, 2013) which revealed that the full extent of the Piccard hydrothermal field comprises 7 polymetallic sulfide mounds, of which 3 actively vent fluids and 4 are inactive (Fig. 1b). Mound locations were confirmed by subsequent mapping, accompanied by mineralogical and geochemical analyses of sulfide minerals (Webber et al., 2015). The sulfide mounds are surrounded by unsedimented pillow basalts and sheet flows with low metalliferous sediment cover. Surficial seafloor geology suggests a classic axial, neovolcanic hydrothermal system hosted in mafic substrate (Kinsey and German, 2013).

Within the Piccard field, high temperature hydrothermal fluids are expelled from two different regions including the Beebe Vents and Beebe Woods areas (Fig. 1c). Venting at Beebe Vents occurs from a linear array of five slender 2–3 m tall focused black smoker chimneys at 4957 m water depth atop a 40 m diameter mound. Venting at Beebe Woods occurs from a cluster of ~10 taller, wider (7 m tall by 0.2–0.5 m wide) beehive diffuser chimneys located on a separate 40 m diameter mound ~100 m south of Beebe Vents at 4962 m depth. The entire Piccard field extends beyond the mounds hosting these high temperature vents, and encompasses a third discrete mound, Beebe Sea, located to the SE of Beebe Vents and NE of Beebe Woods (Fig. 1b). The presence of abundant extinct sulfide chimneys across this 90 m diameter edifice indicates the past occurrence of extensive high temperature venting at the Beebe Sea mound. But currently, only clear, diffuse fluids

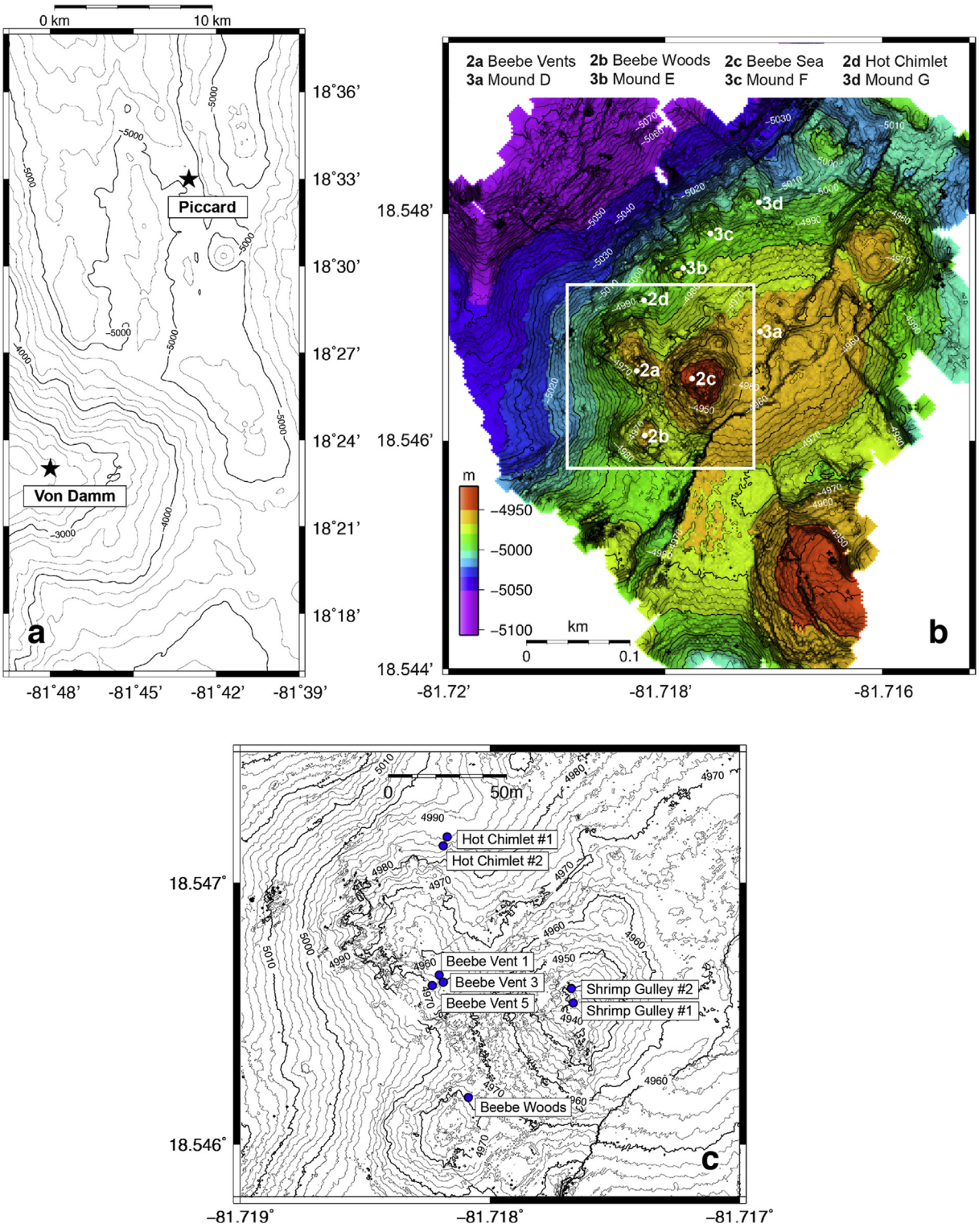

Fig. 1. Maps of the Mid-Cayman Rise (a), the Piccard vent field (b), and inset showing the location of fluid samples (c). Map b shows areas of active venting including the Beebe Vents [2a], Beebe Woods [2b], Beebe Sea [2c], and Hot Chimlet [2d], as well as several hydrothermal sulfide deposits that are inactive, Mounds D [3a], E [3b], F [3c] and G [3d] (modified after Kinsey and German (2013)).

are emitted here, as well as at the Hot Chimlet site (Fig. 1b and c). These low temperature fluid compositions will be discussed in a companion paper.

3. METHODS

3.1. Sample collection

Fluid samples were collected using 150 mL titanium isobaric gas-tight (IGT) samplers (Seewald et al., 2002) deployed by the ROV *Jason II* during R/V *Atlantis* cruise AT18-16 in January 2012 and by the HROV *Nereus* during R/V *Falkor* cruise FK008 in June 2013. Fluid temperatures were monitored continuously during sample collection with a thermocouple aligned with the sampler snorkel inlet. Thermocouples were calibrated with a National Institute of Standards and Technology (NIST) temperature calibrator to an accuracy of ±2 °C. For each fluid sample, the maximum measured temperature (±2 °C) observed during collection is reported (Table 1). Replicate samples were taken at each individual orifice. Samples were extracted and processed within 24 h of sampler recovery on the ship.

During sample processing, aliquots were extracted for immediate shipboard analysis of pH (25 °C) and dissolved CH_4, H_2, CO, and ΣH_2S ($\Sigma H_2S = H_2S + HS^- + S^{2-}$). Further aliquots were archived for shore-based analysis of non-volatile dissolved species (Li, Na, K, Rb, Mg, Ca, Sr, SO_4, Cl, Br, Fe, Mn, Co, Cu, Zn, Pb, Cd, Al, SiO_2), total dissolved inorganic carbon ($\Sigma CO_2 = CO_2 + HCO_3^- + CO_3^{2-}$), dissolved hydrocarbons (C_2H_6, C_3H_8, n-C_4H_{10}, i-C_4H_{10}), total dissolved ammonium ($\Sigma NH_4^+ = NH_3 + NH_4^+$), and total dissolved formate ($\Sigma HCOOH = HCOOH + HCOO^-$). Fluid aliquots for measurement of non-volatile dissolved species were stored in acid-washed high-density polyethylene (HDPE) Nalgene™ bottles. Aliquots for transition metal analysis were immediately acidified to pH <2 with concentrated Optima™ HCl. An aliquot of the acidified transition metal sample was then diluted 100-fold (v/v) and stored for analysis of dissolved SiO_2. A separate fluid aliquot was collected for SO_4 and sparged with N_2 (~20 min) to remove ΣH_2S that may otherwise oxidize during storage and elevate measured SO_4 abundances. Samples for total ammonium species ($\Sigma NH_4 = NH_3 + NH_4^+$) were filtered through 0.2 μm pore size Nylon filters and stored frozen. Aliquots for ΣHCOOH analysis were also stored frozen. Aliquots for shore-based ΣCO_2 abundance and CH_4 and ΣCO_2 stable carbon and radiocarbon isotope analysis were transferred to evacuated serum vials sealed with NaOH-boiled butyl rubber stoppers (Oremland and Des Marais, 1983). Aliquots for trace hydrocarbons were transferred into evacuated glass tubes fitted with Teflon, brass, and stainless gas-tight valves (Cruse and Seewald, 2006). Fluid samples (5 g fluid) for He isotope analysis were transferred under vacuum into evacuated aluminosilicate glass break-seal tubes and flame sealed. Following complete removal of the fluid sample from the IGT sampler, the 'dregs' fraction, which contains precipitates that formed as a result of cooling and mixing within the sampler, was collected at sea on 0.22 μm pore size Nylon filters by rinsing the sample chamber with Milli-Q water and high-purity acetone. The filters were then dried and stored.

3.2. Analytical methods

3.2.1. pH and volatile species

Species abundances determined at sea are reported in units of μmol/L or mmol/L fluid, while those determined on shore are reported in units of nmol/kg, μmol/kg or mmol/kg fluid (Tables 1–3). Fluid pH (25 °C, 1 atm) was measured by potentiometry using a Ag/AgCl combination reference electrode. Dissolved H_2, CH_4, and CO were analyzed by gas chromatography using a 5 Å molecular sieve packed column and thermal conductivity (H_2), flame ionization (CH_4), or helium ionization (CO) detection after headspace extraction in a glass gastight syringe. Dissolved ΣH_2S was determined using two different approaches in 2012. The first involved shipboard analysis by iodometric starch titration of an aliquot drawn into a gastight syringe as described in Von Damm (2000). The second involved precipitation of ΣH_2S as Ag_2S in 5 wt% $AgNO_3$ and storage for later gravimetric determination in a shore-based laboratory following recovery on a 0.22 μm pore size filter. The recovered Ag_2S was stored for subsequent multiple sulfur isotopic analysis. Reported ΣH_2S abundances for 2012 represent an average of results from the titration and gravimetric methods. In 2013 only the titration was performed. For the 2012 samples, ΣCO_2 was determined following sample acidification with 25 wt.% H_3PO_4 by headspace injection into a gas chromatograph equipped with a Porapak™ Q packed column and thermal conductivity detection (Cruse and Seewald, 2006, Reeves et al., 2011). The results are corrected to account for ΣCO_2 partitioning between the fluid and headspace within each serum vial. Samples from 2013 were not processed for ΣCO_2 abundance due to a contamination issue. Trace C_2H_6, C_3H_8, n-C_4H_{10}, and i-C_4H_{10} abundances were determined via a purge-and-trap device interfaced to a gas chromatograph equipped with a Porapak™ Q packed column and flame ionization detection (Cruse and Seewald, 2006) (Table 1). The concentration of ΣNH_4 was determined by flow injection analysis (Hall and Aller, 1992). The analytical uncertainty (2s) was ±0.05 units for pH (25 °C, 1 atm), ±5% for ΣCO_2, CH_4, C_2H_6, C_3H_8, ΣNH_4, and H_2 and ±10% for CO, n-C_4H_{10}, i-C_4H_{10}, and ΣH_2S.

3.2.2. Non-volatile dissolved species

Dissolved non-volatile species concentrations were determined in shore-based laboratories by ion chromatography (IC) (Na, Cl, Ca, K, Li, SO_4, Br, ΣHCOOH), inductively coupled plasma mass spectrometry (ICP-MS) (Mg, SiO_2, Li, Sr, Rb, Fe, Mn, Zn, Cu, Al, Pb, Co, Cd, Ag), and flow injection analysis (ΣNH_4) (Hall and Aller, 1992). Samples were bracketed with NIST-traceable external standards during IC and ICP-MS analysis.

Transition metals readily precipitate upon cooling and mixing in the IGT samplers and subsequent storage. It is therefore necessary to collect and chemically analyze the

Table 1
Measured and calculated endmember vent fluid compositions and isotope values at the Piccard vent field.

Vent (Year)	Sample[a]	T_{max} (°C)	Mg (mm)	pH (25 °C)	Na (mm)	Cl (mm)	Ca (mm)	K (mm)	SiO_2 (mm)	Li (μm)	Rb (μm)	SO_4 (mm)	Br (mm)	Sr (μm)	$^{87}Sr/^{86}Sr$
Beebe Endmember[b]			0	–	314	349	6.18	11.4	20.0	421	5.59	0.21	0.61	21.9	0.70456
Beebe Vent 1	J2-613-IGT1	396	0.96	3.1	316	358	7.23	11.6	19.3	404	5.49	0.74	0.62	23.6	0.70501
(2012)	J2-613-IGT8	398	1.34	3.1	311	352	6.80	11.3	19.0	402	5.46	0.91	0.67	24.1	–
Endmember			0	–	311	351	6.94	11.5	19.5	411	5.57	0.21	0.64	22.4	0.70470
Beebe Vent 3	J2-619-IGT4	394	1.26	3.2	320	354	5.85	11.2	19.6	412	5.53	0.92	0.57	23.1	0.70493
(2012)	J2-619-IGT8	397	1.59	3.2	318	354	5.80	11.2	19.7	415	5.46	1.28	0.53	23.0	–
Endmember			0	–	315	349	5.71	11.2	20.2	424	5.61	0.35	0.54	21.2	0.70451
Beebe Vent 5	J2-613-IGT3	395	2.15	3.0	323	358	6.33	11.5	18.9	415	5.37	1.30	0.66	25.7	–
(2012)	J2-613-IGT4	394	1.29	3.3	317	359	6.04	11.4	20.3	400	5.50	0.89	0.62	23.8	0.70501
Endmember			0	–	315	352	6.05	11.5	20.3	420	5.58	0.18	0.63	22.6	0.70460
Beebe Vent 5	N58-IGT7[h]	390	42.2	5.1	430	499	9.52	10.6	–	105	–	22.4	0.77	–	–
(2013)	N58-IGT8	398	1.60	3.2	319	358	6.50	11.5	–	411	–	1.09	0.62	–	–
Endmember			0	–	314	351	6.40	11.6	–	424	–	0.21	0.62	–	–
Beebe Woods	J2-618-IGT2	352	2.95	3.2	324	341	6.29	11.1	19.6	406	5.40	1.55	0.66	27.3	0.70528
(2012)	J2-618-IGT8	354	2.97	3.2	325	366	5.85	11.2	18.9	400	5.33	1.41	0.61	22.9	–
Endmember			0	–	316	342	5.82	11.2	20.4	425	5.61	-0.11	0.62	21.3	0.70441
Bottom Seawater		~5	52.5	8.0	462	540	10.3	10.4	0.06	26.5	1.24	28.0	0.82	88.5	0.70917

Vent (Year)	Sample[a]	H_2 (mM)	ΣH_2S (mM)	$\delta^{34}S_{H2S}$ (‰)	$\Delta^{33}S_{H2S}$[c] (‰)	ΣNH_4 (μm)	ΣCO_2 (mm)	CO (μM)	ΣHCOOH (μm)	CH_4 (μM)	C_2H_6 (nm)	C_3H_8 (nm)	n-C_4H_{10} (nm)	i-C_4H_{10} (nm)	$\delta^{13}C_{CO2}$ (‰)	$\delta^{13}C_{CH4}$ (‰)	$\delta^{13}C_{C2H6}$ (‰)
Beebe Endmember[b]		19.9	12.0	–	–	–	25.7	–	–	124	–	–	–	–	–	–	–
Beebe Vent 1 (2012)	J2-613-IGT1	18.3	11.5	5.8	-0.030	40.8	25.4[d]	7.7	<1	110	–	–	–	–	-3.8	–	–
	J2-613-IGT8[f]	18.6	11.5	–	–	41.9	25.6	8.5	<1	115	–	–	–	–	-3.9	-23.6	-24.9[e]
Endmember		18.9	11.8	–	–	42.3	26.2	8.3	–	115	–	–	–	–	–	–	–
Beebe Vent 3 (2012)	J2-619-IGT4	20.2	11.9	6.3	-0.004	33.6	25.7	–	<1	120	–	–	–	–	-4.1	–	–
	J2-619-IGT8	20.1	11.5	–	–	33.8	25.0	–	<1	120	10	–	1.2	<0.9	-4.3	-23.8	–
Endmember		20.7	12.0	–	–	34.7	26.0	–	–	123	11	–	1.2	–	–	–	–
Beebe Vent 5 (2012)	J2-613-IGT3	18.4	11.0	–	–	42.0	24.1	7.2	<1	117	15	5.3	2.3	1.2	-4.7	–	–
	J2-613-IGT4[f]	18.8	12.2	–	–	42.5	24.6	7.2	<1	114	14	9.4	2.8	<0.9	-4.8	-24.3	–
Endmember		19.2	12.0	–	–	43.6	25.1	7.4	–	120	15	7.6	2.6	1.3	–	–	–
Beebe Vent 5 (2013)	N58-IGT7	4.13	2.23	–	–	10.2	–	1.8	<1	28.3	–	–	–	–	–	–	–
	N58-IGT8	19.5	12.0	–	–	44.0	–	9.7	<1	130	–	–	–	–	–	–	–
Endmember		20.2	12.3	–	–	45.6	–	10	–	134	–	–	–	–	–	–	–
Beebe Woods (2012)	J2-618-IGT2[f]	19.6	11.4	6.3	-0.020	35.1	24.5	–	4.3	121	28	18	9.0	5.2	–	–	-24.4[e]
	J2-618-IGT8	19.4	11.1	6.0	-0.018	35.0	24.7	–	4.8	120	26	13	5.4	1.2	–	–	–
Endmember		20.7	11.9	–	–	37.2	25.9	–	4.8	128	28	16	7.6	3.4	–	–	–
Bottom Seawater		0	0	–	–	0.1	2.21	0	<1	0	0	0	0	0	–	–	–

[a] Jason (J2) or Nereus (N##) dive number and isobaric gas-tight sampler number (-IGT).
[b] Average high-temperature vent endmember (For Beebe 1, 3, 5, and Beebe Woods).
[c] Measured $\Delta^{33}S_{H2S}$ 1σ errors are: ±0.006 (J2-613-IGT1), ±0.011 (J2-619-IGT4), ±0.007 (J2-618-IGT2), ±0.016 (J2-618-IGT8).
[d] Radiocarbon $\Delta^{14}C$ measurement on vent fluid ΣCO_2 is: Measured Fm = 0.0100 ± 0.0003, Corrected Fm = 0.0085 ± 0.0007 (J2-613-IGT1, #OS-104377).
[e] Multiple samples were combined for $\delta^{13}C_{C2H6}$ values entered for Beebe Vents (J2-613-IGT8, J2-613-IGT1, J2-619-IGT8, J2-613-IGT3) and for Beebe Woods (J2-618-IGT8, J2-618-IGT2).
[f] Measured $^3He/^4He$ (R/Ra) values are: 8.30 ± 0.13 (J2-613-IGT8); 8.37 ± 0.13 (J2-613-IGT4); 8.41 ± 0.13 (J2-618-IGT2). Measured $\Sigma CO_2/^3He$ values are: 6.43E+08 (J2-613-IGT8); 5.45E+08 (J2-613-IGT4); 9.44E+10 (J2-618-IGT2). Note: Although the $^3He/^4He$ ratio for sample J2-618-IGT2 is consistent with a magmatic He source, ^4He abundances that are much lower than the other Beebe Vents suggest that this sample may have leaked prior to analysis. See Table S1 for measured ^4He and calculated ^3He isotope data.

Table 2
Elemental ratios calculated from endmember fluid compositions at the Piccard vent field.

Vent (Year)	T_{max} °C	Mg_{min} [a] (mm)	Na/Cl	K/Cl	Ca/Cl	Sr/Cl ($\times10^{-3}$)	Li/Cl ($\times10^{-3}$)	Rb/Cl ($\times10^{-3}$)	Br/Cl ($\times10^{3}$)	Fe/Cl ($\times10^{-3}$)	Mn/Cl ($\times10^{-3}$)	Fe/Mn	Sr/Ca
Beebe Vent 1 (2012)	398	0.96	0.89	0.033	0.020	0.064	1.2	0.016	1.8	19	1.6	12	3.2
Beebe Vent 3 (2012)	397	1.26	0.90	0.032	0.016	0.061	1.2	0.016	1.6	19	1.6	12	3.7
Beebe Vent 5 (2012)	395	1.29	0.90	0.032	0.017	0.064	1.2	0.016	1.8	18	1.6	12	3.7
Beebe Vent 5 (2013)	398	1.46	0.90	0.033	0.018	–	1.2	–	1.8	–	–	–	–
Beebe Woods (2012)	354	2.95	0.92	0.033	0.017	0.062	1.2	0.016	1.8	37	1.6	23	3.7
Bottom Seawater	~5	–	0.86	0.019	0.019	0.16	0.049	0.0023	1.5	<0.00001	<0.00001	–	8.7

[a] Lowest measured Mg for vent orifice.

solid precipitates so that the fluid composition prior to precipitation can be reconstituted. Small amounts of precipitates formed during storage of acidified metals aliquots were collected by filtration using acid-washed HDPE syringes equipped with removable 0.22 μm Nucleopore™ filters and are termed the 'bottle-filter' fraction. Both the bottle filter and dregs fraction particles were separated from their filters by soaking in 5 mL of reverse *aqua regia* (1:3 HCl: HNO_3) in 30 mL Savillex™ vials overnight (Craddock, 2009). To further digest particulates, uncovered vials were heated at 70 °C until the particles dissolved, and the *aqua regia* was then allowed to evaporate to near dryness. The digestion and dry down process was repeated three times to remove Cl and ensure complete digestion. Digested residues were then dissolved in 5 wt% Optima™ HNO_3 prior to ICP-MS analysis. Analytical uncertainties (2s) were ±3% for Na, Cl, Ca, K, SO_4, Mg, SiO_2 and Sr; ±5% for Li, Rb, Fe, Mn, Zn, Cu, Al, Pb, Co, Cd, ΣNH_4; and ±10% for Br and Ag. See Appendix for ICP-MS analysis methodology details and Tables A2–A4 for metal abundances within each analyzed fraction.

3.2.3. C, S, Sr and He isotopes

Stable carbon isotope (^{13}C) analysis of ΣCO_2, CH_4, C_2H_6 and C_3H_8 was conducted by isotope ratio monitoring-mass spectrometry using a Finnigan Delta-PlusXL mass spectrometer coupled to an Agilent 6890 GC via a GCCIII combustion interface held at 1080 °C with a constant oxygen trickle. The measurement was performed via serum vial headspace injections for ΣCO_2 and CH_4, and a purge-and-trap device for C_2H_6 and C_3H_8. Fluids were acidified with H_3PO_4 prior to ΣCO_2 analysis, and made highly alkaline with NaOH prior to CH_4, C_2H_6, and C_3H_8 analysis to sequester ΣCO_2 in solution. Due to the very low C_2H_6 abundances in the Beebe Vent fluids, it was necessary to combine several sample aliquots collected from multiple orifices and stored in separate glass gas-tight tubes to obtain sufficient carbon for isotopic analysis. This approach is justified by the proximity of the vents and inorganic and organic species abundances that indicate Beebe Vents 1, 3, and 5 share a common endmember composition (see Table 1). Due to variable entrainment of ambient bottom seawater that contains 2.21 mmol/kg ΣCO_2 with a $\delta^{13}C_{CO2}$ value of 1.1‰, reported endmember $\delta^{13}C_{CO2}$ values have been calculated from measured values using an isotope mass balance (Cruse and Seewald, 2006). Measured $\delta^{13}C_{CH4}$, $\delta^{13}C_{C2H6}$, and $\delta^{13}C_{C3H8}$ values are not corrected for seawater mixing since background seawater contains negligible quantities of these hydrocarbons.

Multiple stable sulfur isotope analysis ($\delta^{34}S$, $\delta^{33}S$, $\delta^{36}S$) was conducted on dissolved ΣH_2S in select 2012 samples via isotope ratio mass spectrometry following methods in Ono et al. (2006). Approximately 1 to 2 mg Ag_2S precipitated shipboard from fluid ΣH_2S was reacted under F_2 overnight (~40 torr, 300 °C, 12 + h), and the product SF_6 was purified by gas chromatography prior to isotope ratio analysis by a Thermo-Electron MAT 253.

Carbon and sulfur stable isotope data for each isotope of interest, *A*, are reported in standard delta notation (δA) expressed as:

Table 3
Measured and calculated metal vent fluid compositions at the Piccard vent field.

Vent (Year)	Sample[a]	Al (μm)	Fe (mm)	Mn (μm)	Zn (μm)	Cu (μm)	Pb (μm)	Cd (nm)	Ag (nm)	Co (μm)
Beebe Vent 1 (2012)	J2-613-IGT1	7.1	6.76	549	53.3	197	–	77	177	0.95
	J2-613-IGT8	9.1	6.17	533	51.8	201	–	75	82	0.97
Endmember		8.3	6.61	553	53.7	203	–	78	132	0.98
Beebe Vent 3 (2012)	J2-619-IGT4	7.3	6.52	537	55.0	374	2.8	103	665	0.84
	J2-619-IGT8	6.0	6.46	546	15.5	82.8	0.45	80	–	1.3
Endmember		6.9	6.67	557	36.3	235	1.6	94	682	1.1
Beebe Vent 5 (2012)	J2-613-IGT3	5.4	6.11	534	80.3	130	–	82	115	0.93
	J2-613-IGT4	6.4	6.38	540	65.9	203	0.095	88	51	1.1
Endmember		6.1	6.45	555	75.5	172	0.097	88	85	1.0
Beebe Woods (2012)	J2-618-IGT2	6.7	13.2	525	34.7	616	0.31	50	69	17
	J2-618-IGT8	9.0	10.5	525	52.0	640	0.33	48	65	11
Endmember		8.3	12.5	556	45.9	666	0.34	52	78	15
Bottom Seawater		0	0	0	0	0	0	0	0	0

[a] Jason (J2) or Nereus (N##) dive number and isobaric gas-tight sampler number (-IGT).

$$\delta A(‰) = \left[\frac{R_S - R_{STD}}{R_{STD}}\right] \times 1000 \quad (1)$$

where R_S and R_{STD} are the isotope ratios ($^{13}C/^{12}C$, $^{33}S/^{32}S$, $^{34}S/^{32}S$, $^{36}S/^{32}S$) of the sample and the standard, respectively. Carbon and sulfur stable isotopes are reported relative to the Vienna PDB and Vienna CDT scales, respectively. The pooled standard deviation (2s) for replicate samples was ±0.3‰ for $\delta^{13}C_{CO2}$, ±0.8‰ for $\delta^{13}C_{CH4}$, and the instrumental analytical uncertainty (2s) was ±0.4‰ for $\delta^{13}C_{C2H6}$, ±0.7‰ for $\delta^{13}C_{C3H8}$, and ±0.3‰ for $\delta^{34}S_{\Sigma H2S}$. Sulfur isotope data are additionally expressed in $\Delta^{33}S$ notation, defined as the deviation of the minor isotope ratio from the terrestrial fractionation reference line (Gao and Thiemens, 1991):

$$\Delta^{33}S = \delta^{33}S - 0.515 \times \delta^{34}S \quad (2)$$

Radiocarbon ($^{14}C_{CO2}$) analyses were conducted at the WHOI National Ocean Sciences Accelerator Mass Spectrometry Facility. Results are expressed in terms of Fraction Modern (F_m), representing the deviation of the sample relative to the modern NBS Oxalic Acid I standard (NIST-SRM-4990, AD 1950) (Olsson, 1970). Radiocarbon contents were corrected to remove the effects of seawater mixing using the same approach that was used to correct $\delta^{13}C_{CO2}$ values. Measured analytical uncertainties are listed in Table 1. Corrected radiocarbon F_m uncertainties are conservative estimates calculated via error propagation of independent variables that accounts for the effects of [Mg] and [ΣCO_2] analytical uncertainties.

Selected fluid samples were analyzed for He abundance and isotope composition in the Isotope Geochemistry Facility at WHOI. Helium was cryogenically separated from the other noble gases (Lott, 2001), and analyzed as described in German et al. (2010). The procedural line blank is $<1.5 \times 10^{-9}$ cc STP ^{4}He. One full procedural blank, which included the sea-going extraction line and full storage time in the break seal tube, was $\sim 6 \times 10^{-9}$ cc STP ^{4}He (with atmospheric $^3He/^4He$). These blank levels are insignificant relative to the samples (<3‰ in all cases). Uncertainties for ^{4}He abundances are approximately ±5% due to splitting procedures.

Strontium isotopic analysis was conducted on selected samples. Conventional ion-exchange procedures with Sr specific resin were used to separate and collect Sr, and $^{87}Sr/^{86}Sr$ isotope ratios were measured with a ThermoFinnigan NEPTUNE multi-collector inductively coupled plasma-mass spectrometer as described in Voss et al. (2014) and corrected for potential Rb and Kr interferences as described by Jackson and Hart (2006). The internal precision for Sr isotopic measurements is ±0.000010 (2σ). The external precision, after correction to values for NBS987 (0.710240) is ±0.000025 (2σ).

3.3. Calculation of endmember fluid compositions

Experimental, theoretical, and field studies have shown that hydrothermal fluids undergo near quantitative removal of Mg and SO_4 during fluid-rock reaction with basalt and gabbro at high temperatures (>300 °C) and low water/rock ratio (Bischoff and Dickson, 1975; Mottl and Holland, 1978; Seyfried and Bischoff, 1981; Von Damm et al., 1985). Accordingly, the presence of measureable quantities of dissolved Mg in high temperature ridge-crest hydrothermal fluids can be attributed to the dead-volume of the IGT samplers (~4 ml), which are pre-filled with bottom seawater prior to deployment, and inadvertent entrainment of ambient seawater during sample collection. Sampled fluid compositions are assumed to reflect two-component mixing of a zero-Mg 'endmember' fluid with bottom seawater. The compositions of zero Mg endmembers prior to mixing were calculated via least-squares regression of an individual conservative chemical species as a function of Mg for all samples from one vent orifice, weighted to pass through bottom seawater composition and extrapolated to 0 mmol/kg Mg.

Due to non-conservative behavior during fluid-seawater mixing, endmember pH was not calculated by extrapolation to zero-Mg, but rather the minimum measured pH (25 °C,

1 atm), corresponding to the lowest Mg fluid, is reported. Endmember $^{86}Sr/^{87}Sr$ values were calculated by a linear extrapolation to a zero molar Mg/Sr ratio (Albarède et al., 1981).

4. RESULTS

4.1. Temperature, Mg, and pH

High temperature black smoker Beebe Vents 1, 3 and 5 emitted focused, low-Mg fluids with nearly identical temperatures in 2012 and 2013 that ranged from 390–398 °C (Table 1), significantly below the temperatures required for phase separation at Piccard seafloor pressures (Bischoff and Rosenbauer, 1985). A maximum temperature of 354 °C was measured at Beebe Woods in 2012 after removal of a beehive diffuser to expose a well-defined orifice for sampling.

High temperature fluids at Piccard were acidic, with pH (25 °C, 1 bar) values that ranged from 2.9 to 3.1 in all low-Mg Beebe Vent and Beebe Woods fluids in 2012, and 3.2 in the low-Mg sample from Beebe Vent 5 in 2013 (Table 1).

4.2. Dissolved non-volatile species

Fluids at Beebe Vents 1, 3, and 5 and Beebe Woods sampled in 2012 are characterized by nearly identical endmember concentrations of Cl, SiO_2, SO_4, Na, Br, Ca, Sr, K, Li, and Rb, suggesting that the high temperature regions of the Piccard vent field are fed by a common source fluid. Endmember values for fluids collected from Beebe Vents in 2013 match the 2012 values, indicating that fluid composition did not change during the one-year time span between sampling occasions (Table 1). The high temperature source fluid feeding the Piccard vents is depleted in Cl by ~35% relative to seawater, with an average endmember concentration of 349 mmol/kg (Fig. 2a). The endmember Na concentration is 314 mmol/kg, a value that is ~32% lower than seawater (Fig. A1a). Dissolved SiO_2 abundance is greatly enriched relative to seawater in the endmember fluids, with a concentration of 20.0 mmol/kg (Fig. 2b). Aqueous SO_4 abundances decrease linearly with respect to Mg to near-zero concentrations in endmember fluids (0.21 mmol/kg) (Fig. A1b). Endmember Br, Ca, and Sr concentrations are also depleted relative to seawater with concentrations of 0.61 mmol/kg, 6.18 mmol/kg, and 21.9 μmol/kg, respectively (Table 1; Fig. A1c, 2c, A1d). The concentrations of alkali metals K, Li and Rb are all higher than seawater, with endmember abundances of 11.4 mmol/kg, 421 μmol/kg and 5.59 μmol/kg, respectively (Figs. A1e, A1f, 2d).

Because Cl is the dominant anion in vent fluids, and charge balance constraints dictate that changes in Cl require changes in dissolved cations, it is common practice to normalize elements to Cl to allow for identification of enrichments or depletions in vent fluid species relative to the starting seawater composition. The endmember vent fluid is characterized by Na/Cl and Ca/Cl ratios that are very similar to those of seawater, in contrast with the higher ratios observed for Br/Cl, K/Cl, Li/Cl, and Rb/Cl and the lower ratio observed for Sr/Cl (Table 2). The endmember $^{87}Sr/^{86}Sr$ isotopic composition is 0.70456, consistent with the known global range for hydrothermal fluids (Albarède et al., 1981; Ravizza et al., 2001) (Fig. 3).

4.3. Volatile aqueous species

Vents at Beebe Vents 1, 3, and 5 and Beebe Woods are characterized by nearly identical endmember values for the dissolved concentrations of H_2, ΣH_2S, ΣCO_2, CO, and CH_4, further reinforcing the interpretation that the high temperature regions of the Piccard vent field are fed by a single source fluid (Table 1). The Piccard endmember H_2 abundance is 19.9 mmol/L (Fig. 4a), substantially higher than H_2 contents previously observed at other non-eruptive mafic-hosted vent fields, where concentrations are typically <1 mmol/L H_2 (e.g., Welhan and Craig, 1983; Merlivat et al., 1987; Evans et al., 1988; Proskurowski et al., 2008; Charlou et al., 1996). Piccard endmember ΣH_2S content is 12.0 mmol/L and is similar to abundances observed at other basalt-hosted high temperature vents (Fig. 4b). Likewise, high temperature $\delta^{34}S_{H2S}$ values of +5.8 to +6.3‰ are within previously observed ranges (Shanks, 2001; McDermott et al., 2015a) (Table 1). High temperature fluid $\Delta^{33}S_{H2S}$ values of −0.004 to −0.030‰ are near zero, indicating normal mass-dependent fractionation, similar to what is observed in other black smoker fluids (McDermott et al., 2015a).

Endmember ΣCO_2, CO, and CH_4 concentrations are 25.7 mmol/kg, 8.5 μmol/L, and 124 μmol/L respectively (Fig. 5a–c), similar to values observed in other unsedimented basalt-hosted black smoker systems (Merlivat et al., 1987; Charlou et al., 1996). Endmember $\delta^{13}C_{CO2}$ values in Beebe Vents 1, 3 and 5 and Beebe Woods, range from −4.8 to −3.8‰ (Table 1), and fall within the spectrum anticipated for degassing of ΣCO_2 from basaltic magmas (Pineau and Javoy, 1983). Measured $\delta^{13}C_{CH4}$ values are similar in all Piccard black smoker fluids, ranging from −23.6 to −24.3‰ (Table 1). These values are slightly depleted in ^{13}C relative to other unsedimented basalt hosted black smoker vent fluids, where $\delta^{13}C_{CH4}$ values range from −9 to −20‰ (e.g., Welhan and Craig, 1983, Merlivat et al., 1987; Proskurowski et al., 2008; Charlou et al., 1996). Endmember C_2H_6, C_3H_8, n-C_4H_{10}, and i-C_4H_{10} abundances range from 1.2 to 15 nmol/kg at Beebe Vents 3 and 5, with slightly higher concentrations at Beebe Woods that range from 3.4 to 28 nmol/kg (Figs. 5d, A2a and A2b). At each vent, hydrocarbon abundance decreases with increasing chain length. The combined $\delta^{13}C_{C2H6}$ value of -24.9‰ for the Beebe Vent 1, 3, and 5 samples (see Methods section) matches the Beebe Woods $\delta^{13}C_{C2H6}$ value of −24.4‰ (Table 1).

Fluid $\Delta^{14}C_{CO2}$ values are near the detection limit in Beebe Vent 1 (Table 1). Dissolved formate species ($\Sigma HCOOH = HCOOH + HCOO^-$) are below detection (<1 μmol/kg) in Beebe Vents 1, 3 and 5, but are quantifiable in the Beebe Woods fluid, which contains an endmember ΣHCOOH abundance of 4.8 μmol/kg (Table 1). The isotopic composition of He in the Piccard vent fluids indicates R/R_a values of 8.30–8.41 (Tables 1 and A1) which are consistent with a mantle source (Craig and Lupton, 1976;

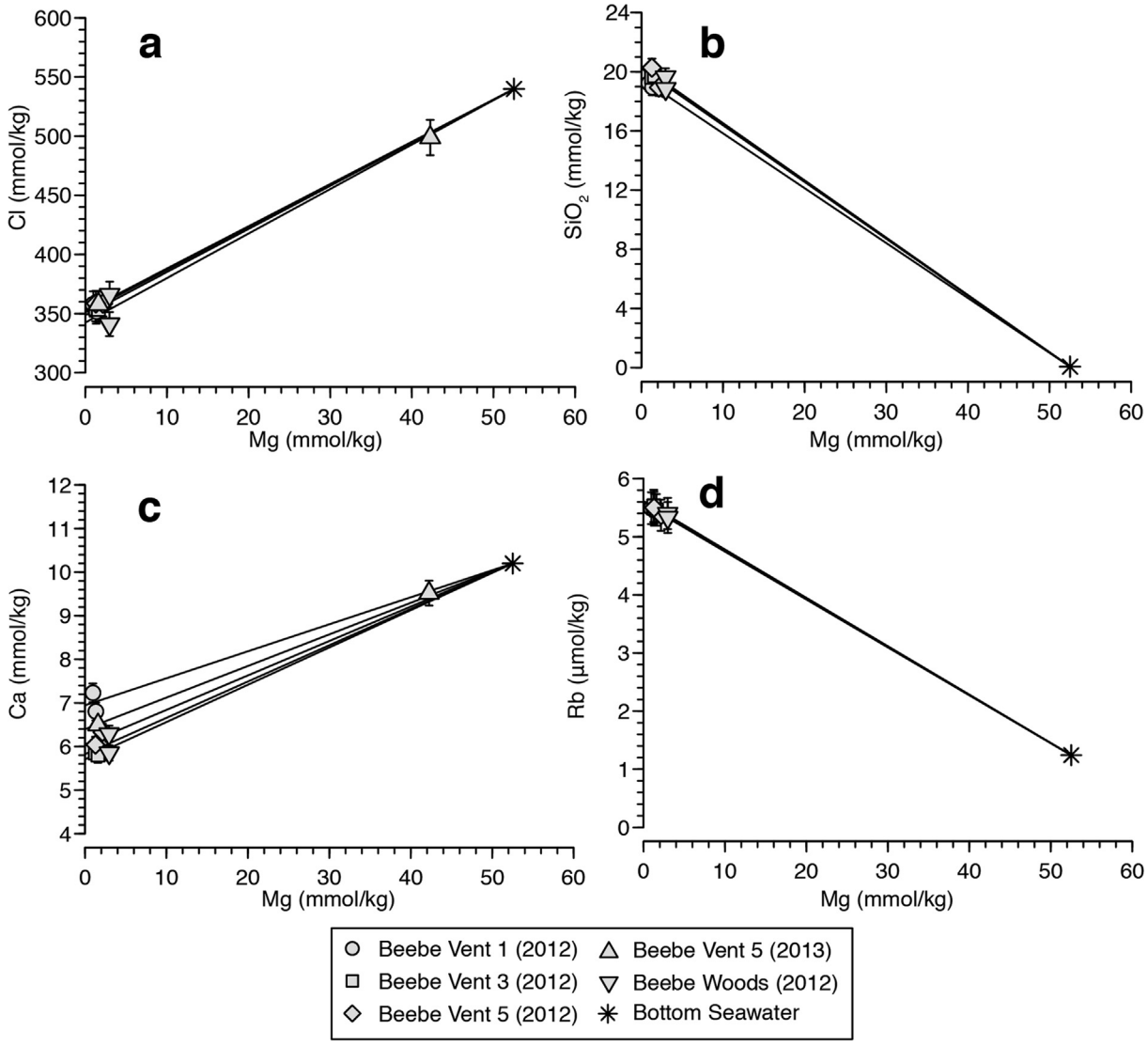

Fig. 2. Measured concentrations of Mg versus Cl (a), SiO_2 (b), Ca (c) and Rb (d) for hydrothermal fluids sampled at the Piccard vent field in 2012 and 2013. The extrapolated zero-Mg endmembers for the high temperature fluids are indicated by the lines. 2 s errors are shown, or are smaller than the symbols.

Lupton and Craig, 1975). Measured $\Sigma CO_2/^3He$ ratios in Beebe Vents 1 and 5 of 5.45 to 6.43 $\times$ 10^8 are just below the average R/Ra ratio of 1 $\times$ 10^9 measured in mantle rocks (Marty and Tolstikhin, 1998).

4.4. Transition metals

Dissolved transition metals in Piccard high temperature fluids are highly enriched relative to seawater abundances. In general, reported concentrations for dissolved transition metals in submarine hot springs are characterized by relatively high and variable degrees of uncertainty due to the inadvertent entrainment of dislodged chimney particles during sampling and precipitation of metals within the fluid sampler. Beebe Vents 1, 3, and 5 fluids are characterized by Fe endmember abundances ranging from 6.45 to 6.67 mmol/kg and Mn abundances ranging from 553 to 557 µmol/kg (Table 3, Fig. 6a and b). Endmember abundances for Cu and Zn range from 172 to 235 µmol/kg and 53.7 to 75.5 µmol/kg (Fig. 6c and d). Endmember Pb contents range from 0.097 to 1.6 µmol/kg, Co ranges from 0.98 to 1.1 µmol/kg, Ag ranges from 85 to 682 nmol/kg, and Cd ranges from 78 to 94 nmol/kg. Data for the abundance of Al likely reflect contamination during sample handling, due to the abundance of Al in commonly used lab supplies. The measured Al values are therefore presented as maxima.

Beebe Woods fluids are characterized by large enrichments of some metals relative to the Beebe Vents (e.g., Fe, Cu, Co), while other metals have similar concentrations (e.g., Mn). Beebe Woods likely shares the same source fluid as the Beebe Vents, since almost every other aspect of fluid chemistry is similar. Due to the friable nature of the beehive chimney surrounding the Beebe Woods vent, entrainment of pyrite and chalcopyrite particles into the fluid likely

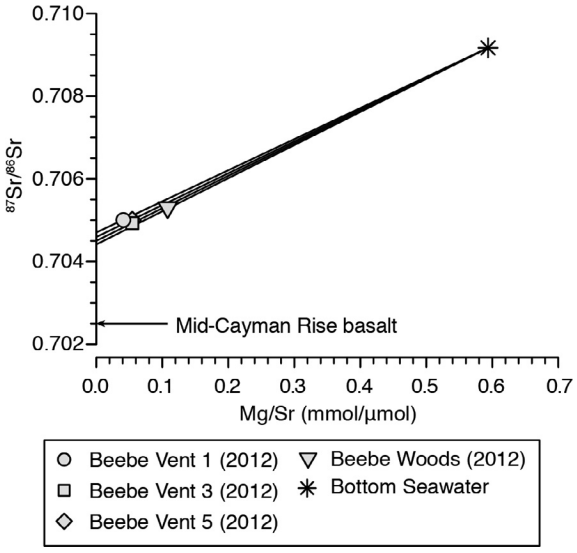

Fig. 3. Measured Mg/Sr versus $^{87}Sr/^{86}Sr$ for selected hydrothermal fluids at the Piccard vent field. The extrapolated zero-Mg/Sr endmembers for the high temperature fluids are indicated by the lines. The average $^{87}Sr/^{86}Sr$ ratio for basalt from the Mid-Cayman Rise is indicated by the arrow (Cohen and O'Nions, 1982). 2 s errors are smaller than the symbols.

occurred, resulting in elevated concentrations of some metals in the 'dregs' fraction. In support of this interpretation, the metal enrichments at Beebe Woods are primarily observed in the 'dregs' fraction, (Table A4), while the 'dissolved' and 'filter' fractions do not have substantially elevated metal contents relative to Beebe Vent 1, 3 and 5 (Tables A2 and A3). It is likely, therefore, that measured metal abundances at Beebe Woods reflect entrainment of particulates, rather than a true difference in endmember source composition. Accordingly, only the Beebe Vents metal concentrations are discussed below.

5. DISCUSSION

5.1. Formation of endmember 'black smoker' fluids

Piccard vent fluids share common formation characteristics with high temperature convective deep-sea hydrothermal systems worldwide. Within this framework, the effects of the higher pressure that sets the site apart can be discerned. The composition of ridge-crest hydrothermal fluids reflects the cumulative influence of a variety of factors, including bottom seawater composition, the composition of the rock through which the fluid circulates, the depth of circulation, and the nature of the heat source. These last two factors determine the pressure and temperature conditions of water-rock reaction and establish whether or not the fluid reaches the two-phase boundary, triggering phase separation (Bischoff and Rosenbauer, 1985; Driesner and Heinrich, 2007; Fig. 7). Seawater descends through permeable rock within the 'recharge' zone, first undergoing lower temperature chemical reactions. Further reactions occur during progressive heating with increasing depth, until fluids attain their highest temperature and maximum buoyancy and ascend to the seafloor in upflow zones. The net effect is the transformation of seawater into a Mg- and SO_4-poor, slightly acidic, anoxic fluid that is enriched in alkalis, Ca, SiO_2, metals, H_2S, and ΣCO_2 (Alt, 1995; Von Damm, 1995; German and Seyfried, 2014).

The Piccard hydrothermal field is surrounded by basaltic seafloor outcrops and situated atop a spur of lava domes (Kinsey and German, 2013; Webber et al., 2015). These

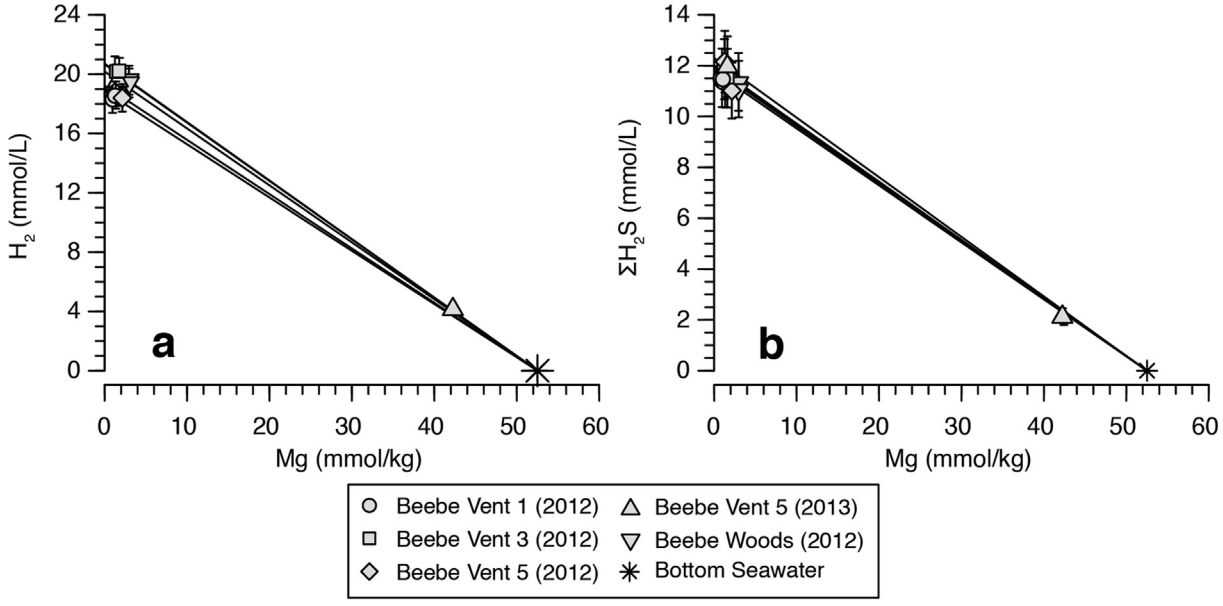

Fig. 4. Measured concentrations of Mg versus H_2 (a) and ΣH_2S (b) for hydrothermal fluids sampled at the Piccard vent field in 2012 and 2013. The extrapolated zero-Mg endmembers for the high temperature fluids are indicated by the lines. 2 s errors are shown, or are smaller than the symbols.

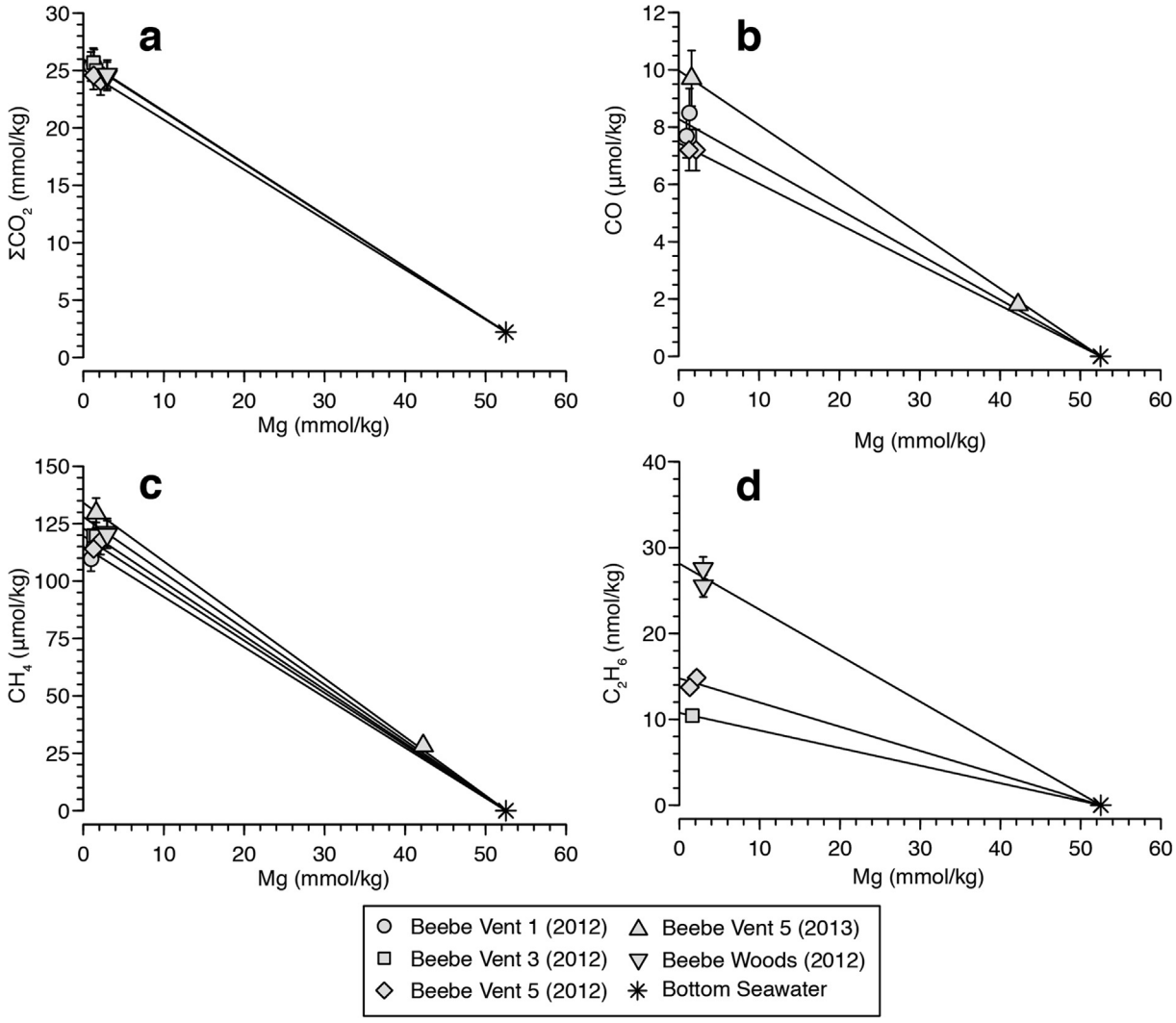

Fig. 5. Measured concentrations of Mg versus ΣCO_2 (a), CO (b), CH_4 (c), and C_2H_6 (d) for hydrothermal fluids sampled at the Piccard vent field in 2012 and 2013. The extrapolated zero-Mg endmembers for the high temperature fluids are indicated by the lines. 2 s errors are shown, or are smaller than the symbols.

observations, along with the neovolcanic axial location of the vent field, point to the likely involvement of basalt and gabbros during the water-rock reactions that regulate fluid chemistry at the Piccard vent field. Due to the thin crust along ultramafic ridges in general, however, including that inferred from gravity modeling across the Mid-Cayman Rise (2–3 km, ten Brink et al., 2002) additional interaction with ultramafic lithologies cannot be precluded.

5.1.1. Phase separation

All of the high temperature endmember fluids venting at Piccard contain Cl contents that are significantly lower than seawater, with an average endmember concentration of 349 mmol/kg. Due to the lack of a major sink for Cl within mafic-hosted subsurface circulation pathways, Cl depletions in vent fluids are typically attributed to phase separation (Von Damm, 1990, 1995; Foustoukos and Seyfried, 2007b). Thus, the large Cl depletions observed in the Beebe Vents and Beebe Woods endmember fluids, in conjunction with a seafloor pressure of 496 bar that places the two-phase boundary at 483 °C, suggests that they have experienced phase separation at conditions that are both hotter and deeper (higher pressure) than the critical point for seawater at 407 °C and 298 bar (Bischoff, 1991). During incipient phase separation from supercritical seawater, a small amount of high-salinity brine condenses to form a separate phase, creating a Cl-depleted residual fluid, or vapor phase. The Cl-depleted fluids venting at Piccard represent this vapor phase. Although a vent fluid of seawater chlorinity is not a supercritical fluid at the conditions of seafloor venting (398 °C, 496 bar), the Piccard vent fluids represent a supercritical phase owing to their lower chlorinity (Bischoff, 1991; Bischoff and Pitzer, 1989). Phase relations in the system NaCl-H_2O can be used to estimate the minimum temperature of phase separation based on the chlorinity of the vapor phase and the assumption that phase separation occurs at or below the seafloor. Examination of Fig. 7 reveals that a minimum temperature of 491 °C is

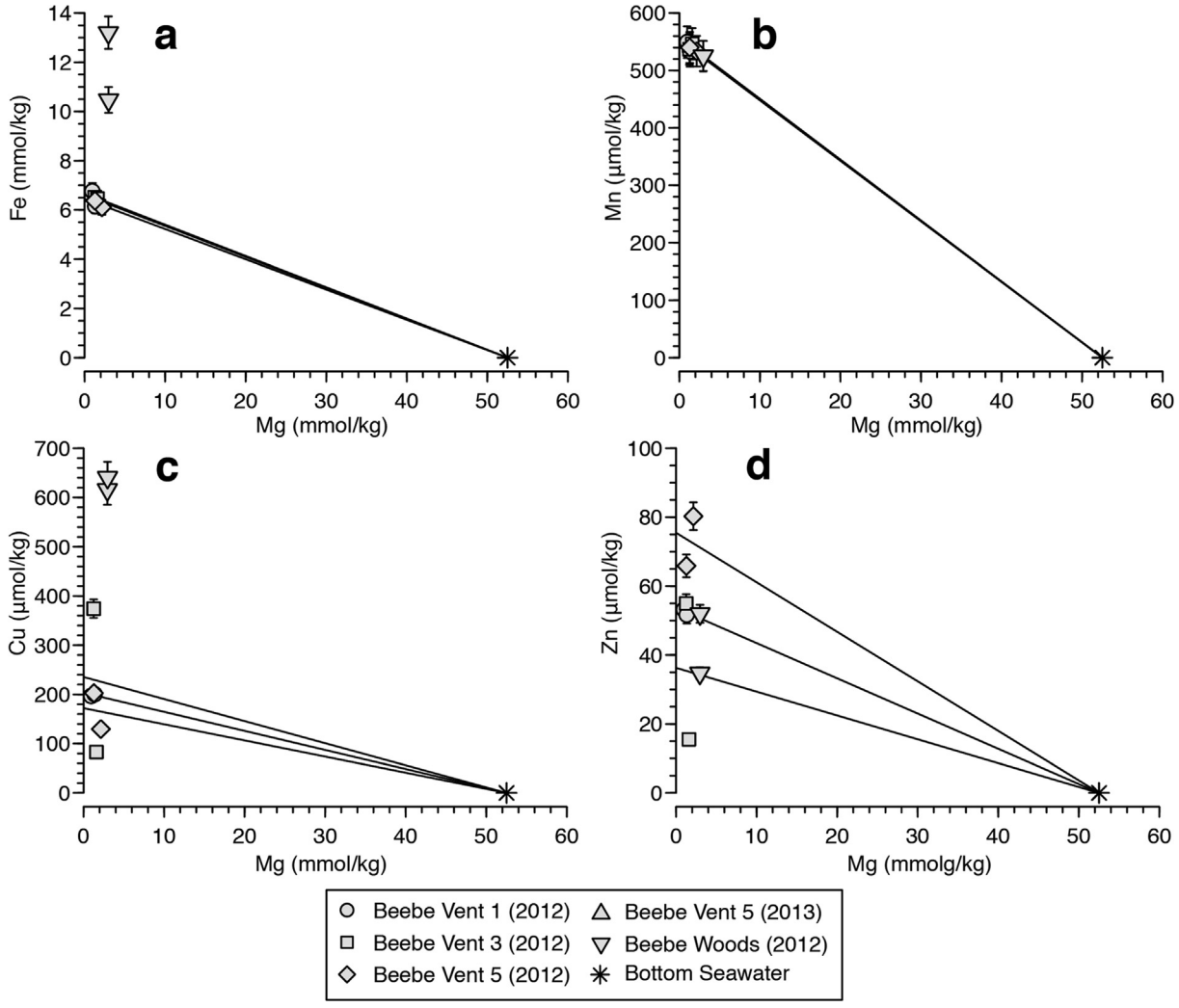

Fig. 6. Measured concentrations of Mg versus Fe (a), Mn (b), Cu (c), and Zn (d) for hydrothermal fluids sampled at the Piccard vent field in 2012. Note that the elevated Fe, Cu, and Zn abundances in Beebe Woods relative to Beebe Vent fluids are likely the result of sampling artifacts (see text). The extrapolated zero-Mg endmembers for the high temperature fluids are indicated by the lines. 2 s errors are shown, or are smaller than the symbols.

required to produce the measured Cl concentration of 349 mmol/kg observed in the Beebe Vents endmember fluids. Accordingly, the observed Cl depletion in the high temperature endmember fluids at Piccard indicates that these fluids must have cooled by at least 90 °C prior to venting, and perhaps more. For example, if the location of phase separation was 1000 m deeper, then that would require maximum fluid temperatures in the vicinity of 535 °C (Fig. 7).

Elevated Br/Cl ratios at Beebe Vents and Beebe Woods relative to seawater are also consistent with phase separation under supercritical conditions. Laboratory experiments have shown that Br partitions equally between vapor and liquid phases during subcritical phase separation (Berndt and Seyfried, 1997), but fractionates preferentially into the vapor phase during supercritical phase separation producing an increase in vapor phase Br/Cl ratios (Berndt and Seyfried, 1990; Foustoukos and Seyfried, 2007a). Chloride normalized partition coefficients defined by the expression:

$$D_{\mathrm{Br/Cl}} = \frac{(M_{\mathrm{Br}}/M_{\mathrm{Cl}})_{\mathrm{v}}}{(M_{\mathrm{Br}}/M_{\mathrm{Cl}})_{\mathrm{b}}} \quad (3)$$

where $(M_{\mathrm{Br}}/M_{\mathrm{Cl}})_{\mathrm{v}}$ and $(M_{\mathrm{Br}}/M_{\mathrm{Cl}})_{\mathrm{b}}$ represent the Br/Cl molal concentration ratio in the vapor and brine, respectively (Berndt and Seyfried, 1990; Foustoukos and Seyfried, 2007a), can be used to express the fractionation of Br relative to Cl between vapor and brine during phase separation. It has been shown that vapor-brine partition coefficients for Br increase systematically with decreasing water density according to the expression:

$$\log D_{\mathrm{Br/Cl}} = -13.04 - 54.95(\log \rho_{\mathrm{w}}) - 76.93(\log \rho_{\mathrm{w}})^2 - 36.09(\log \rho_{\mathrm{w}})^3 \quad (4)$$

where ρ_{w} represents the density of pure water (Foustoukos and Seyfried, 2007a).

Owing to the systematic variation of water density as a function of temperature and pressure, Eq. (4) can be used

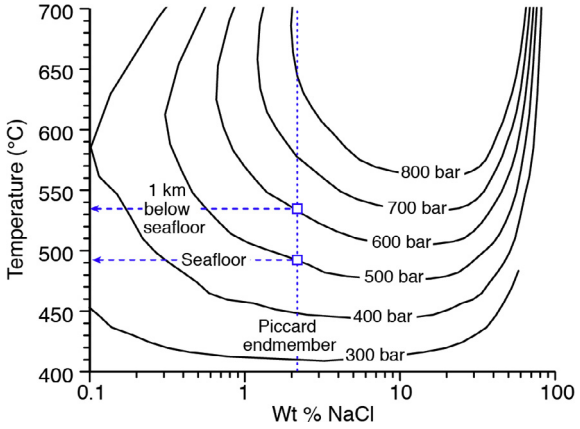

Fig. 7. Isobars of the vapor-liquid region of NaCl-H_2O from 300 to 800 bar (Foustoukos and Seyfried, 2007b). The Piccard endmember wt.% NaCl is indicated with a dotted vertical line, and the pressures at the seafloor and 1 km below seafloor are indicated with dashed horizontal lines at 491 °C and 535 °C, respectively.

to constrain conditions of phase separation if values $D_{Br/Cl}$ for a given fluid are known. The composition of the brine phase at Piccard is unknown, precluding calculation of $D_{Br/Cl}$ for Piccard vent fluids. Minimum values of $D_{Br/Cl}$ can be determined, however, if it is assumed that seawater represents the only source of Br and Cl since mass balance constraints require that Br/Cl ratios in the brine be lower than the starting seawater that produced Br-enriched vapors. Measured Br/Cl ratios (μmol/mmol) at Piccard vary from 1.6 to 1.8 representing a 5 to 18% increase relative to the starting seawater value of 1.5, and yield minimum values of $D_{Br/Cl}$ that vary from 1.1 to 1.2 with corresponding water densities (ρ_w) during phase separation that vary from 0.229 to 0.247 g/ml according to Eq. (4). For phase separation occurring at a seafloor pressure of 500 bar, temperatures of 506 to 518 °C are required to produce water densities of this magnitude while phase separation occurring 1000 m below the seafloor at a pressure of 600 bar requires temperatures from 555 to 573 °C. Thus, enrichment of Br relative to Cl in the vapor phase venting at Piccard is consistent with supercritical phase separation at temperatures in excess of 500 °C and provides additional evidence for substantial cooling of Piccard hydrothermal fluids prior to venting. Although halite precipitation during phase separation can also generate elevated Br/Cl ratios in a vapor phase due to exclusion of Br from the halite crystal structure (Stoessel and Carpenter, 1986; Stoessel, 1992; Berndt and Seyfried, 1997; Foustoukos and Seyfried, 2007a), phase relations in the system NaCl-H_2O limit the coexistence of halite and a vapor phase during phase separation of seawater to pressures lower than ~400 bar. Accordingly, halite precipitation cannot be responsible for elevated Br/Cl ratios at Piccard (Bischoff, 1991; Driesner and Heinrich, 2007).

5.1.2. Fluid-mineral equilibria

The dissolved SiO_2 content of high temperature mafic-hosted hydrothermal fluids can be used to estimate the depth (pressure) and temperature of water-rock reaction if it is assumed that fluids equilibrate with quartz in subseafloor reaction zones and do not re-equilibrate during rapid ascent through the discharge zone to the seafloor (Bischoff and Rosenbauer, 1985; Von Damm et al., 1991). Because quartz solubility varies systematically as a function of temperature and pressure, either parameter can be estimated if the other is known. Examination of Fig. 8 reveals that the SiO_2 content of the fluids Beebe Vents and Beebe Woods would be in equilibrium with quartz at 400 bar and at 500 bar, respectively, at the measured vent temperatures. The Beebe Vents could not have equilibrated with quartz at the measured vent temperatures since this would require a pressure of just 400 bar, placing the reaction zone 1000 m *above* the seafloor. Models for the formation of the Piccard vent fluids that involve fluid-quartz equilibria require that the fluids equilibrated with quartz at temperatures substantially higher than the measured seafloor values and subsequently cooled prior to venting. Because quartz solubility at temperatures above ~350 °C and low pressure is characterized by retrograde temperature dependence, equilibrium pressures of ≥500 bar that place the reaction zone at or below the seafloor at Piccard require temperatures in excess of the measured 398 °C to produce the observed aqueous SiO_2 concentrations (Fig. 8). For example, the 20 mmol/kg dissolved SiO_2 in endmember fluids at Beebe Vent and Beebe Woods would be consistent with equilibrium with quartz at temperatures just over 450 °C for a seafloor pressure of 500 bar (Fig. 8). Although quartz solubility in seawater salinity fluids has not been determined at temperatures >450 °C, existing data for solubility trends as a function of temperature and pressure imply substantially higher temperatures that exceed 500 °C, if fluid-quartz equilibria is occurring 1000 m below the seafloor at a pressure of 600 bar (Von Damm et al., 1991; Fontaine et al., 2009). Thus, the temperatures inferred from dissolved SiO_2 contents and quartz geothermometry are consistent with the temperatures required for supercritical phase separation.

Because Cl is the dominant anion in vent fluids, charge balance constraints result in a positive correlation between the concentrations of cations and chlorinity. Although the partitioning of cations between vapor and brine phases during supercritical phase separation is not uniform (Berndt and Seyfried, 1990; Foustoukos and Seyfried, 2007a), normalization of cation abundances to chloride allows qualitative comparison of cation abundances between hydrothermal fluids that have experienced variable degrees of phase separation. Na/Cl ratios at Piccard are within the range observed for vent fluids from other unsedimented basalt-hosted mid-ocean ridge hydrothermal systems (Gallant and Von Damm, 2006). In contrast, Ca/Cl ratios are among the lowest ever observed at non-eruptive basalt-hosted vent fields (Table 2, Fig. 9). Laboratory experiments and theoretical studies have shown that the Na and Ca content of ridge crest hydrothermal fluids is controlled by pressure and temperature-dependent thermodynamic equilibrium with plagioclase and epidote solid solutions in basalt-hosted systems (Seyfried and Ding, 1995; Berndt and Seyfried, 1993; Berndt et al., 1989;

Seyfried et al., 1991). In particular, with increasing temperature, the greater stability of the anorthite and clinozoisite components of plagioclase and epidote solid solutions according to the reactions:

$$Ca^{2+} + \underset{\text{albite}}{2NaAlSi_3O_{8(s)}} = \underset{\text{anorthite}}{CaAl_2Si_2O_{8(s)}} + 2Na^{+} + 4SiO_{2(aq)} \quad (5)$$

$$Ca^{2+} + \underset{\text{anorthite}}{3CaAl_2Si_2O_{8(s)}} + 2H_2O_{(l)} = \underset{\text{clinozoisite}}{2Ca_2Al_3Si_3O_{12}(OH)_{(s)}} + 2H^{+} \quad (6)$$

results in increased Ca-fixation and reductions in the Ca/Cl ratio of hydrothermal vent fluids.

Whether or not plagioclase-epidote equilibria represents an appropriate model to account for the chemistry of Piccard vent fluids is presently unclear since laboratory and theoretical studies of fluid-basalt interaction at temperature in excess of 500 °C have not been conducted. Nonetheless, comparison of Ca/Cl ratios at Piccard with ratios in vent fluids from other basalt-hosted systems indicates some of the lowest values observed to date (Fig. 9), consistent with high temperatures of fluid-rock interaction in subseafloor reaction zones estimated from other geochemical indicators. The low Ca/Cl ratios indicate removal of Ca from solution and formation of Ca-bearing secondary minerals. While plagioclase-epidote solid solutions may represent likely candidates, the higher temperatures estimated for Piccard may also move the fluids into the stability field for Ca-bearing amphiboles.

Water/rock mass ratios (w/r) during formation of the Piccard vent fluids can be estimated using abundances of the alkali elements Li and Rb, and Sr abundance and isotopic composition. Experimental and field studies demonstrate that the alkali elements are highly mobile during fluid/rock reaction, and are nearly quantitatively leached from the rock during high temperature basalt alteration (Mottl and Holland, 1978; Seyfried et al., 1984; Von Damm, 1990; Von Damm et al., 1985). Indeed, K, Li, and Rb abundances in the Piccard vent fluids are enriched relative to seawater. If it is assumed that Li and Rb are leached quantitatively from basalt of known Li and Rb content, and that these species are not partitioned into any secondary mineral phases, then a w/r ratio can be calculated (e.g., Von Damm et al., 1985). Mid-Cayman Rise basalt contains 1.92 ppm Rb according to a single measurement of an axial basalt (Cohen and O'Nions, 1982). Although the Li content of Mid-Cayman Rise basalts is unknown, a recent study of axial basalts dredged from 13–14°N MAR reports 6.11 ppm Rb and 5.11 ppm Li (n = 109) (Wilson et al., 2013). The larger sample set in that study may better reflect the average composition of basalt erupted at slow and ultraslow spreading centers. Average endmember fluid Rb contents (5.59 μmol/kg) yield w/r ratios of 5 (for 1.92 ppm Rb in rock) to 16 (for 6.11 ppm Rb in rock) for the range of rock Rb concentrations, while average endmember fluid Li contents (422 μmol/kg) yield a w/r ratio of 2.

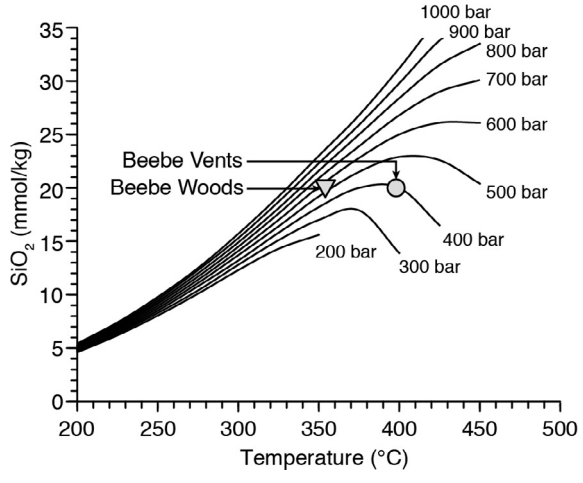

Fig. 8. Plot of aqueous SiO_2 concentrations in equilibrium with quartz as a function of temperature and pressure (Von Damm et al., 1991). The symbols show the measured aqueous SiO_2 and maximum measured temperature of the Beebe Vents 1, 3, 5 and Beebe Woods.

The isotopic composition of Sr ($^{87}Sr/^{86}Sr$) in endmember hydrothermal fluids represents an effective means to estimate w/r ratios because Sr isotopes do not fractionate during precipitation or dissolution reactions (Berndt et al., 1988). Vent fluid Sr content typically correlates with Ca, as reactions involving Ca-bearing primary and secondary mineral phases also control Sr abundances (Berndt et al., 1988). The Piccard Sr concentration is depleted relative to seawater, although still within the range observed at high temperature mid-ocean ridge systems (Gallant and Von Damm, 2006), and the Sr/Cl ratio indicates that fluids have lost dissolved Sr during fluid/rock reaction on a seawater-normalized basis. An average endmember $^{87}Sr/^{86}Sr$ ratio of 0.70456 calculated for the low Mg endmember fluids is consistent with a predominantly rock source of Sr (Fig. 3). Berndt et al. (1988) describe a model in which the evolution of Sr abundance and isotopic composition in hydrothermal fluids can be modeled in the context of incomplete Sr removal by anhydrite precipitation in the recharge zone (substitution for Ca) and simultaneous addition of Sr from dissolution of Ca- and Sr-bearing plagioclase minerals during high temperature fluid/rock reaction.

Application of the simultaneous dissolution and precipitation model developed by Berndt et al. (1988) permits calculation of a w/r ratio that is parameterized by simultaneous release of rock-derived Sr and precipitation of Sr into secondary mineral phases. The bulk Sr content of Mid-Cayman Rise basalts is similar to other mid-ocean ridge basalt values worldwide, with an average abundance of 192 ppm (Cohen and O'Nions, 1982; Elthon et al., 1995) and $^{87}Sr/^{86}Sr$ ratio of 0.7025 (Cohen and O'Nions, 1982; Fig. 3). For these values, w/r ratios of 30 to 50 are estimated for Piccard vent fluids (Fig. 10). These values are higher than the w/r ratios calculated based on the alkali elements, but this difference is not unusual (Berndt et al., 1988). The difference in w/r ratios arises due to differences in the geochemical behavior of these elements during rock crystallization and subsequent hydrothermal alteration. For example, the alkali metals are relatively incompatible

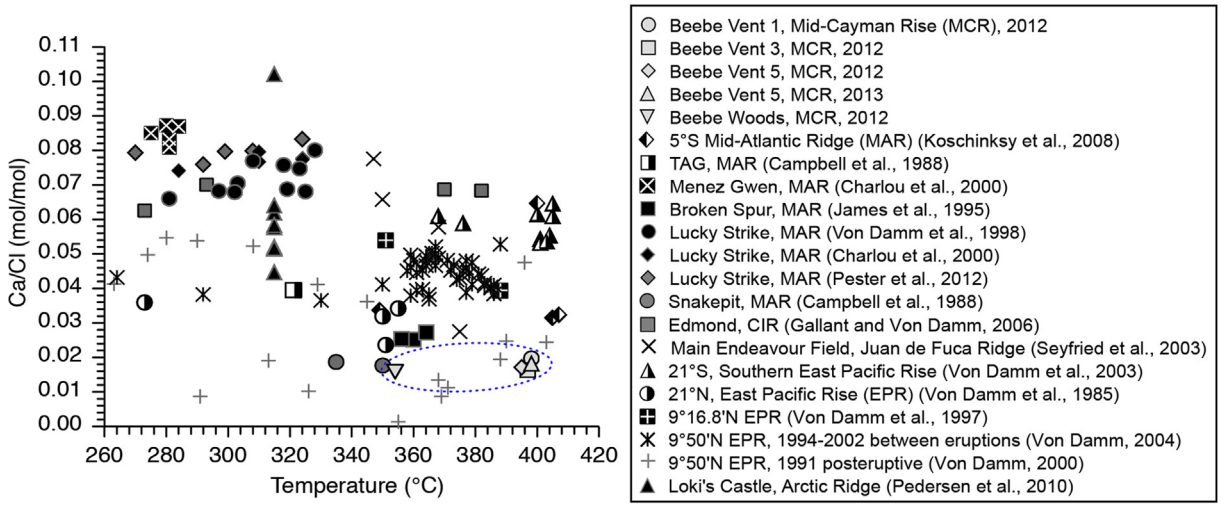

Fig. 9. Measured fluid Ca/Cl ratios at Beebe Vents and Beebe Woods (within blue dotted ellipse), relative to those at basalt-hosted mid-ocean ridge vent fields worldwide. (For interpretation of the references to colour in this figure legend, the reader is referred to the web version of this article.)

during igneous mineral formation and are concentrated in glasses and interstitial material. During hydrothermal alteration, alkali metals are readily leached from unstable phases and only minimally impacted by incorporation into secondary minerals. In contrast, Sr is concentrated in plagioclase during primary mineral formation and readily incorporated into Ca-rich phases formed during hydrothermal alteration (Berndt et al., 1988). The alkali metal w/r ratios therefore provide a sense for the amount of alkali-containing minerals or glass altered, while w/r ratios derived from Sr indicate the extent of plagioclase alteration. The w/r ratios for Li, Rb, and Sr at Piccard are higher than those calculated for most basalt-hosted systems, where ratios between 1–2 are more typical for Li and Rb, and a ratio of ~10 is more typical for Sr (e.g., Von Damm et al., 1985; Butterfield and Massoth, 1994; Butterfield et al., 1997; Kadko and Butterfield, 1998; Foustoukos and Seyfried, 2005). The relatively high mass of water relative to rock can account for the very low fluid K contents at Piccard.

5.1.3. Dissolved metals

An empirical Fe/Mn geothermometer developed for basalt-hosted hydrothermal fluids up to temperatures of 450 °C (Pester et al., 2011) is based upon the experimentally demonstrated temperature sensitivity of the precipitation reactions that control Fe and Mn solubility. Dissolved metal abundances in black smoker fluids are influenced by pH and the stability of metal-chloro complexes, which are pressure and temperature dependent. Among the highest abundance metals in hydrothermal vent fluids, temperature-dependent rates of equilibration with sulfide minerals are fastest for Cu, followed by Fe, Zn, and finally Mn (Seewald and Seyfried, 1990). At Piccard, fluid chemistry indicates that higher temperature fluids share a common source. Application of the empirical geothermometer at Piccard predicts a subsurface temperature of 452 °C for Beebe Vents 1, 3, and 5. Although this inferred temperature is higher than the measured vent temperatures, a result consistent with cooling prior to venting, it is substantially lower than other geochemical indicators described above that indicate temperatures far in excess of 491 °C. The discrepancy may reflect application of the Pester et al. (2011) geothermometer beyond the calibration range. Alternatively, this result may suggest that fluid Fe/Mn ratios have been affected by fluid cooling at Piccard, and it is likely that the fluids have lost Fe, as well as ΣH_2S, to sulfide precipitation after attaining their highest temperature, and then cooling, prior to venting at the seafloor.

Piccard fluids have cooled extensively from their highest temperatures, a common observation made in field and experimental studies of axial systems where fluids attain higher temperatures at depth (often 375–400 °C) and then lose heat prior to venting at the seafloor at temperatures that are lower by at least 20–30 °C (Berndt et al., 1989; Seewald and Seyfried, 1990; Seyfried, 1987). It is therefore expected that dissolved Cu and Fe contents at Piccard would decrease more quickly due to a decrease in temperature, while Zn and Mn contents would be slower to respond and are more likely to record high temperature concentrations.

A study by Pester et al. (2014) showed that at 9°50′N East Pacific Rise (EPR), hydrothermal fluids venting during volcanic eruptions have higher Fe/Mn ratios and lower Mn/Cl ratios than those during steady-state interim non-eruptive periods. These changes were attributed to shifts in the affinity of each metal for low chlorinity vapor phase fluids due to changes in pressure and temperature and the conditions of phase separation (Pester et al., 2014). Relative to Fe, higher temperatures are needed to promote complexation of Mn with Cl allowing it to enter the vapor phase. Due to the higher pressure in the Piccard system relative to 9°50′N EPR, such behavior of Fe and Mn would require substantially higher temperatures. The dissolved Fe/Mn ratio in fluids varies systematically as a function of the solvent properties of water. These solvent properties are a function of the dielectric constant of water, hence we can use this property to compare Piccard results with those of the Pester study. The dielectric constant of H_2O under the

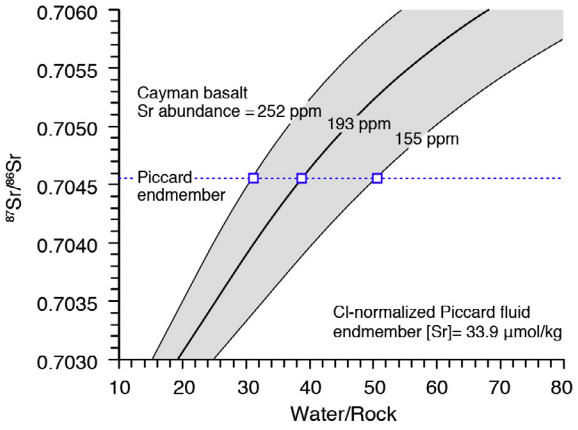

Fig. 10. Plot of hydrothermal fluid Sr isotope composition as function of water/rock mass ratio and Sr abundance in the Mid-Cayman Rise basalt protoliths (Cohen and O'Nions, 1982; Elthon et al., 1995). At Piccard, dissolved Sr abundances and $^{87}Sr/^{86}Sr$ ratios in the Beebe Vents endmember fluid indicate a w/r mass ratio between 30 and 50 (blue open squares). This variability is due to variation of bulk Sr in the basalt, which can range from 155 to 252 ppm, and averages 193 ppm (Cohen and O'Nions, 1982; Elthon et al., 1995). (For interpretation of the references to colour in this figure legend, the reader is referred to the web version of this article.)

relatively lower temperature and pressure experimental conditions of the Pester study (410–465 °C, 220–400 bars) is nearly equivalent to the dielectric constant of H_2O at the relatively higher inferred Piccard reaction temperature and pressure (~535 °C, 600 bar) (Fernández et al., 1997). Hence analogous complexation behavior of Fe and Mn would be expected. Indeed, the endmember fluid Mn/Cl ratios at Beebe Vents fall within the 'eruptive' range of vent chemistries observed at 9°50′N EPR, as does the Fe/Mn ratio (Table 2), consistent with the effects of high temperature reactions.

Among the highest temperature vent fluids measured worldwide, the Turtle Pits and Sisters Peak vents at 5°S MAR have low Fe/Cu ratios that are most similar to the observed ratios of 28 to 38 in Beebe 1, 3 and 5 (Fig. 11). The abundance of Cu and Fe in circulating deep-sea hydrothermal vent fluids is controlled by temperature-dependent metal complexes in NaCl-dominated fluids, and on Fe and Cu-bearing mineral solubility. The ratio of dissolved Fe/Cu (mol/mol) has been proposed as a potential indicator of fluid redox and temperature conditions, provided pH and Cl conditions are well constrained (Seyfried and Ding, 1993; Seyfried and Ding, 1995). Piccard fluids have likely cooled substantially from ≥500 °C temperatures; thus previous studies that investigated Fe and Cu dynamics at temperatures ≤400 °C provide contextual information but cannot be applied directly. During fluid cooling, dissolved metals would be precipitated as pyrite (FeS_2) and chalcopyrite ($FeCuS_2$). Fluid Fe and Cu abundances would decrease with decreasing temperature, and experimental and thermodynamic modeling studies show that decreases in Cu exceed those of Fe, such that the Fe/Cu ratio of the fluid increases as a function of progressive cooling (Seewald and Seyfried, 1990; Seyfried and Ding, 1993, 1995). The observed Fe/Cu ratios of 28 to 38 in Beebe 1, 3, and 5 can be considered maximum values that are consistent with a high temperature origin of these fluids, but do not necessarily reflect reaction zone conditions (Table 2). That these values are still relatively low, compared with theoretical models, experimental observations, and field measurements (Fig. 11) is consistent with high temperatures of fluid-rock reaction, and reflects the high Cu contents of the Beebe Vents fluids (172–232 µmol/kg).

5.1.4. Aqueous H_2 and H_2S

A striking feature of vent fluid chemistry at Piccard is the very high aqueous H_2 content of the high temperature endmember fluids. The observed endmember concentration of 19.9 mmol/L greatly exceeds typical H_2 concentrations of <1 mM in non-eruptive basalt hosted MOR systems (e.g., Welhan and Craig, 1983; Merlivat et al., 1987; Evans et al., 1988; Proskurowski et al., 2008; Charlou et al., 1996) and is higher than abundances observed at many ultramafic-influenced systems, such as Von Damm, Rainbow, and Lost City (Charlou et al., 2002, 2010; Proskurowski et al., 2008; McDermott et al., 2015b). Dissolved H_2 concentrations are regulated by fluid-mineral equilibria and phase separation processes during high temperature, high-pressure seawater-mafic substrate alteration, and both effects must be considered at Piccard. In mafic-hosted hydrothermal systems, H_2 abundances are buffered by equilibration with Fe-bearing oxides, sulfides, and aluminosilicate minerals (Seyfried and Ding, 1995; Seyfried et al., 2003). During phase separation, dissolved volatiles will preferentially partition into the low salinity vapor phase fluid (Seyfried and Ding, 1995). The effects of phase separation alone are likely insufficient to explain the observed H_2 enrichment at Piccard because other volatile species such as CH_4, ΣH_2S, and ΣCO_2 are not similarly enriched relative to other hydrothermal systems.

It is possible that the exceptionally high temperatures of fluid/rock reaction facilitated by the great depth of the Mid-Cayman Rise axis are responsible for the high dissolved H_2 abundances. Basalt alteration studies suggest that pyrite-pyrrhotite-magnetite (PPM) or hematite-magnetite (HM) mineral assemblages likely bracket the range of redox conditions in natural systems (Seyfried and Ding, 1995; Seyfried et al., 1991; Seewald and Seyfried, 1990). With increasing temperature, H_2 contents in equilibrium with these buffers increase. Although laboratory experiments constraining redox during mafic alteration at these conditions are currently lacking for subsurface conditions likely to exist at Piccard, thermodynamic data for the stability of the PPM and HM mineral assemblages can be used to assess temperature conditions during formation of the Piccard vent fluids. If equilibration with the HM buffer is assumed in deep-seated reaction zones, the observed Piccard H_2 concentrations indicate a temperature of 579 °C (Fig. 12a). Equilibration with the PPM redox buffer would require substantially lower temperatures to account for the observed H_2 concentrations, but the Piccard ΣH_2S abundances are well below equilibrium values for PPM at all temperatures >400 °C (Fig. 12b), suggesting

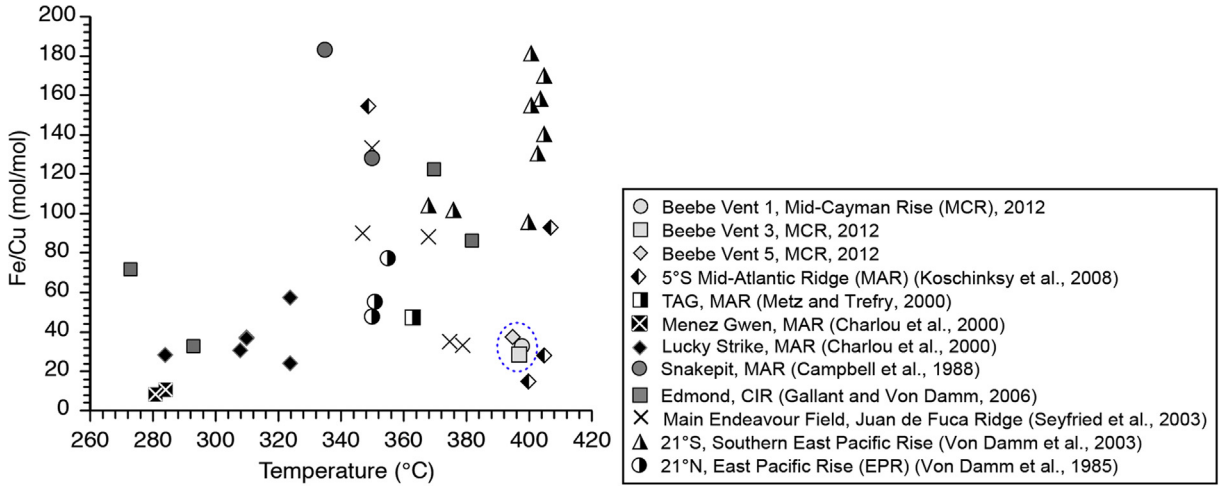

Fig. 11. Measured fluid Fe/Cu ratios at Beebe Vents (within blue dotted ellipse), relative to those determined at basalt-hosted mid-ocean ridge vent fields worldwide. (For interpretation of the references to colour in this figure legend, the reader is referred to the web version of this article.)

that unless large amounts of H_2S have precipitated during cooling, ΣH_2S and H_2 concentrations are not buffered by the PPM assemblage. Similarly, although H_2 may be buffered by HM at high temperatures, ΣH_2S is substantially below that required for HMP equilibria (Fig. 12b). This finding may be a consequence of the relatively high w/r ratio at Piccard that limits rock-derived H_2S, thereby preventing saturation of the fluids with sulfide minerals. Aqueous H_2 concentrations may also be regulated by redox dependent aluminosilicate mineral assemblages, as has been suggested for basalt-hosted hot-springs with reaction zone temperatures in the vicinity of 400 °C (Seyfried and Ding, 1995). These assemblages buffer H_2 at concentrations between PPM and HM in the ~400 °C systems, suggesting that if similar processes are regulating H_2 at the Piccard vents, temperatures lower than the 579 °C estimated from the HM buffer are likely.

Dissolved ΣH_2S abundances of 12.0 mM in the Beebe Vents and 11.9 mM in Beebe Woods are elevated relative to the endmember ΣH_2S contents of other basalt-hosted black smoker systems on the slow spreading Mid-Atlantic Ridge, such as TAG, Snakepit, and Lucky Strike where concentrations range from 0.6 to 6.0 mmol/L (Douville et al., 2002), and point to high temperatures of water-rock reaction at Piccard. Although concentrations of dissolved ΣH_2S are strongly influenced by redox conditions and Cl concentrations, temperature is also an important variable with increasing temperatures during fluid/rock reaction resulting in higher fluid ΣH_2S contents (Seyfried and Janecky, 1985; Seyfried and Ding, 1995; Seyfried et al., 2003).

Sulfur isotope analysis of vent fluid ΣH_2S shows a narrow range of $\delta^{34}S$ values (+5.8‰ to +6.3‰). Major contributors to ΣH_2S in vent fluids at unsedimented mid-ocean ridge hydrothermal systems include basalt-derived sulfide (pyrite and pyrrhotite) of mantle origin, with an average $\delta^{34}S$ value of $+0.1 \pm 0.5$‰ (Sakai et al., 1984), and reduction of seawater SO_4, with an initial $\delta^{34}S$ value of $+21.0 \pm 0.2$‰ (Rees et al., 1978). Piccard $\delta^{34}S_{H2S}$ values suggest that seawater SO_4 persisting into the reaction zone underwent reduction to ΣH_2S via oxidation of rock-derived sulfide (Shanks and Seyfried, 1987; Woodruff and Shanks, 1988). At Piccard, endmember fluid $\delta^{34}S$ values reflect contributions of mantle-derived sulfur that varied from 72 to 70% relative to seawater-derived sulfur contributions of 28 to 30%.

Precipitation of pyrite, presumably formed during fluid cooling and ascent to the seafloor, presents an alternative mechanism that may contribute to the high H_2 contents in Piccard black smoker vent fluids. The following calculations explore this idea first from the observed fluid H_2 budget, and second, from the inferred Fe loss during cooling from higher temperatures. Pyrite precipitation generates H_2 and acidity, while consuming dissolved Fe and H_2S:

$$Fe^{2+} + 2H_2S_{(aq)} = FeS_{2(s)} + 2H^+ + H_{2(aq)} \quad (7)$$

If pyrite precipitation during fluid cooling were responsible for the entire 19.9 mM H_2 content observed in Beebe Vents and Beebe Woods endmember fluids, then an equivalent amount of Fe would have been lost, along with 38.8 mM H_2S during ascent of the high temperature fluid. If measured Mn endmember abundances are assumed to be conservative during fluid ascent due to sluggish reaction kinetics for Mn precipitation (Seewald and Seyfried, 1990), then extrapolation of the empirical Fe/Mn geothermometer by Pester et al. (2011) to 520 °C would predict a reaction zone fluid Fe content of 26.5 mmol/kg. Note that similar Fe concentrations that averaged 23.1 mmol/kg were observed in basalt-seawater alteration experiments conducted at 500 °C, 1000 bars (n = 7; Mottl et al., 1979). Comparing the extrapolated value of 26.5 mmol/kg with the measured fluid Fe contents of 6.45 to 6.67 mmol/kg produces an Fe deficit of ~ 19.9 mmol/kg. Hence, if fluids attained temperatures of ~520 °C, then sufficient Fe could have been lost to pyrite formation to generate the observed H_2. Pyrite precipitation to this extent would also generate

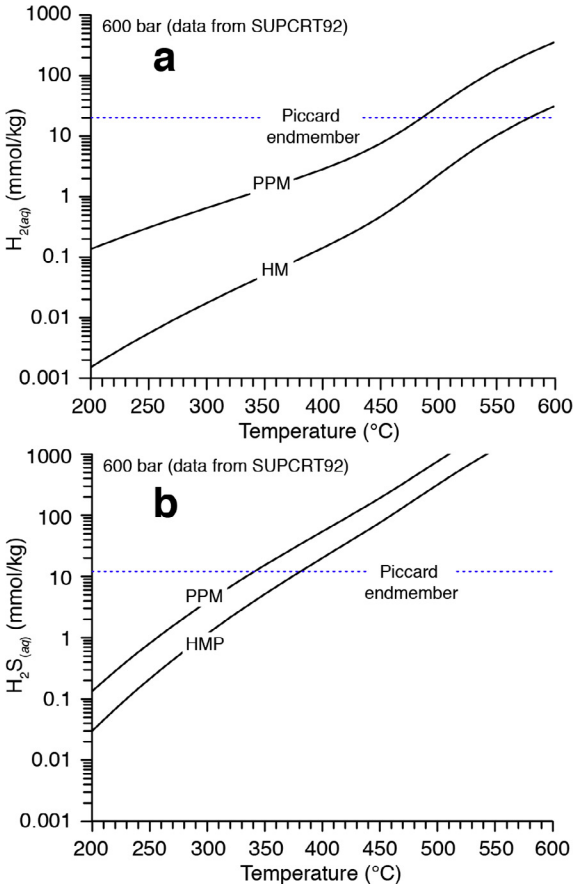

Fig. 12. $H_{2(aq)}$ abundances at thermodynamic equilibrium (a) with the pyrite-pyrrhotite-magnetite (PPM) and hematite-magnetite (HM) buffers at 600 bar as a function of temperature (solid black lines), calculated from standard molal thermodynamic properties with the SUPCRT92 software package (Johnson et al., 1992). Measured $H_{2(aq)}$ abundances at the Piccard black smoker vents (dotted blue line) are consistent with equilibrium HM at temperatures of 579 °C, providing a high-end constraint on subsurface reaction temperatures. Calculated $H_2S_{(aq)}$ abundances at thermodynamic equilibrium (b) with the PPM and hematite-magnetite-pyrite (HMP) are shown as function of temperature at 600 bar (black solid lines; Johnson et al., 1992). Measured $H_2S_{(aq)}$ abundances at the Piccard black smoker vents (dotted blue line) are well below equilibrium at inferred subsurface reaction temperatures, indicating that fluid $H_2S_{(aq)}$ contents are not controlled by buffering with PPM or HMP at depth. (For interpretation of the references to colour in this figure legend, the reader is referred to the web version of this article.)

acidity corresponding to ~1.4 pH units, however, a value that is substantially lower than the observed range of 3.0 to 3.2. If pyrite precipitation is responsible for the elevated H_2 at Piccard, the cooled fluid would have had to have undergone reaction with a highly albitized upflow zone, which would buffer pH and only contribute Na to fluids. If the upflow were not albitized, then a large release of Ca or K would have been observed, in order to balance such a large amount of titrated acidity. Thus, the more plausible model to generate the observed high H_2 abundances at Piccard is likely the one in which it is generated by high temperature reaction between fluid and mafic substrates.

5.1.5. Dissolved carbon species

Piccard fluid ΣCO_2 abundances are consistent with a direct contribution of magmatic volatiles, and are similar to previous studies of basalt-hosted MORs in which ΣCO_2 origins are attributed to active magmatic degassing (Lilley et al., 2003; Seewald et al., 2003). Piccard vent fluid ΣCO_2 $\delta^{13}C$ values of −4.8 to −3.8‰ (Table 1) fall within the observed range of basaltic magmatic degassing (Pineau and Javoy, 1983). Dissolved $^3He/^4He$ ratios at Piccard are also consistent with a mantle source (Tolstikhin and Marty, 1998) which could be derived either from magmatic volatile-rich fluid inclusions, as is postulated at Von Damm (McDermott et al., 2015b) or from active magmatic degassing. Measured $\Sigma CO_2/^3He$ ratios of 5.45 to 6.43×10^8 are just below the average value for $\Sigma CO_2/^3He$ measured in mantle rocks (1×10^9) (Marty and Tolstikhin, 1998) and further support a mantle source for high temperature ΣCO_2 (Table A2). Finally, a radiocarbon-dead ^{14}C ΣCO_2 measurement in Beebe Vent 1 also supports a mantle source for ΣCO_2 (Table 1).

The origin of CH_4 and longer-chained (C_{2+}) hydrocarbons in hydrothermal systems has been of interest since their discovery due to the potential role of abiotic hydrocarbon production in natural settings in the origin and sustenance of life (e.g., Shock, 1990, 1992; Macleod et al., 1994; Martin et al., 2008; Russell et al., 2010) and as a source of metabolic energy and carbon to support microbiological communities inhabiting the sub-seafloor, seafloor, and overlying water column (e.g., Baross and Deming (1995); Huber et al., 2007 Dick et al., 2013). Possible sources of CH_4 and longer chained hydrocarbons in black smoker hydrothermal fluids such as those at Piccard include thermal decomposition of particulate and dissolved organic carbon (DOC, POC) to CH_4 and C_{2+} hydrocarbons. This organic substrate may be derived from the seawater source fluid (~40 μmol/kg DOC and ~0.1 μmol/kg POC in the deep Atlantic Ocean (Druffel et al., 1992; Hansell and Carlson, 1998)) and/or decomposition of vent-associated biomass. An additional potential source is the degassing of mantle-derived CH_4, in a process akin to degassing of ^3He (Lupton and Craig, 1975). Finally, abiotic organic synthesis of CH_4 and C_{2+} hydrocarbons from ΣCO_2 and H_2 may occur, either within magmatic volatile-rich fluid inclusions and gas-rich vesicles within the lithosphere that is undergoing alteration (Kelley and Früh-Green, 1999; Kelley et al., 2002; McDermott et al., 2015b), or during active hydrothermal fluid circulation in high-H_2 systems (Welhan, 1988; Charlou et al., 2002; Foustoukos and Seyfried, 2004; Seyfried et al., 2004; McCollom and Seewald, 2007; Proskurowski et al., 2008).

Chemical disequilibria between ΣCO_2 and CH_4 have been observed in other basalt-hosted black smoker systems that contain lower dissolved H_2 than Piccard. In these systems, CH_4 excesses relative to equilibrium with ΣCO_2 are ubiquitous, and carbon isotope equilibration points to CH_4 formation temperatures that are significantly greater

than vent fluid temperatures (Welhan and Craig, 1983; Seyfried et al., 2004; McCollom and Seewald, 2007; Proskurowski et al., 2008). Carbon isotope fractionation between ΣCO_2 and CH_4 at Beebe Vents 1, 3, and 5 and Beebe Woods is ~19.7‰, a value consistent with isotopic equilibrium at $\sim 393^{+19}_{-5}$ °C (Horita, 2001), close to the measured vent temperatures. This result is unexpected given the well-known kinetic barriers to reversible ΣCO_2-CH_4 equilibrium and molal abundance ratios of $CH_4/\Sigma CO_2$ that are two orders of magnitude away from thermodynamic equilibrium for the reaction:

$$CO_{2(aq)} + 4H_{2(aq)} = CH_{4(aq)} + 2H_2O_{(l)} \quad (8)$$

at measured vent H_2 abundance, temperature and pressure (Shock et al., 1989). Due to the strong temperature dependence of reaction 8, however, the measured concentrations of CH_4, ΣCO_2, and H_2 would be consistent with equilibrium at 430 °C, a value that is near the 398 °C measured vent temperature, but substantially below the maximum temperatures estimated in deep-seated reaction zones. Equilibration of CH_4 and ΣCO_2 at near-seafloor conditions at Piccard is unlikely in light of observations that other chemical parameters (e.g., SiO_2) do not re-equilibrate upon cooling of the fluid during ascent. Accordingly, the significance of the apparent isotopic equilibration temperatures is unclear. The relative abundance of CH_4 and ΣCO_2 may be regulated by kinetic barriers, as has been postulated for other hydrothermal systems such as Rainbow, Logatchev, and Von Damm (Seyfried et al., 2004; McDermott et al., 2015b). The source of CH_4 at Piccard is equivocal, but may involve a combination of thermogenic sources (pyrolysis of seawater-derived DOC or biomass) and leaching of abiotic CH_4 contained in fluid inclusions (Kelley and Früh-Green, 1999; McDermott et al., 2015b).

Other carbon species at Piccard show patterns of chemical equilibration. Experimental findings have demonstrated rapid equilibrium kinetics of the water gas shift reaction:

$$CO_{2(aq)} + H_{2(aq)} = CO_{(aq)} + H_2O_{(l)} \quad (9)$$

For example, at 350 °C (a typical temperature for black smoker vents), the calculated half-life for CO oxidation via reaction 9 is of the order of two minutes (Seewald et al., 2006). At other unsedimented ultramafic and basalt-hosted systems, such as Rainbow, 21°N East Pacific Rise, and 9°50′N EPR, calculated affinities for reaction (Eq. (9)) in hot source fluids are all within or near equilibrium (Seewald et al., 2006; Reeves et al., 2014), as are affinities at the Main Endeavour Field (Foustoukos et al., 2009). Consistent with rapid kinetics observations and field observations, calculated affinities for reaction 9 at measured conditions and compositions of Piccard high temperature fluids are also all near equilibrium (+5.0 to +5.5 kJ/mol).

At the nearby Von Damm vent field at the Mid-Cayman Rise, reducing conditions, coupled with the lower temperatures and higher pH conditions, provide a thermodynamic drive for the abiotic reduction of ΣCO_2 by H_2 to ΣHCOOH (McDermott et al., 2015b), according to the reaction:

$$CO_{2(aq)} + H_{2(aq)} = HCOO^- + H^+ \quad (10)$$

The calculated chemical affinity for reaction 10 at Beebe Woods is −2.6 kJ/mol, a value within ±5 kJ/mol of zero affinity. This finding is consistent with thermodynamic equilibrium between the metastable species ΣCO_2, H_2, and ΣHCOOH, and thereby provides support for an abiotic origin of ΣHCOOH at Beebe Woods (Shock and Helgeson, 1990) (see Appendix for calculation details). The observation that ΣHCOOH is below detection (<1 μmol/kg) in the Beebe Vents is also consistent with thermodynamic equilibrium of Eq. (10), determined for the relatively higher maximum measured temperature of 398 °C. Equilibration of Beebe Woods fluids, which share the same ΣCO_2, H_2, and pH composition as Beebe Vents, at relatively lower temperatures of venting (354 °C) promotes measureable ΣHCOOH production in the Beebe Woods fluids.

Longer chained alkanes in the Piccard endmember fluids, C_2H_6, C_3H_8, n-C_4H_{10}, and i-C_4H_{10}, are present at nanomolar levels that are four to five orders of magnitude lower than endmember CH_4 abundances. The origin of the C_{2+} hydrocarbons is presently unclear, but may involve a deep abiotic source or, more likely, thermogenic alteration of the abundant biomass that is in close proximity to submarine hot-springs. Indeed, the beehive chimney-associated Beebe Woods fluids contain substantially higher C_2H_6, C_3H_8, and n-C_4H_{10} than the Beebe Vents, despite other chemical indicators that support a shared deep source

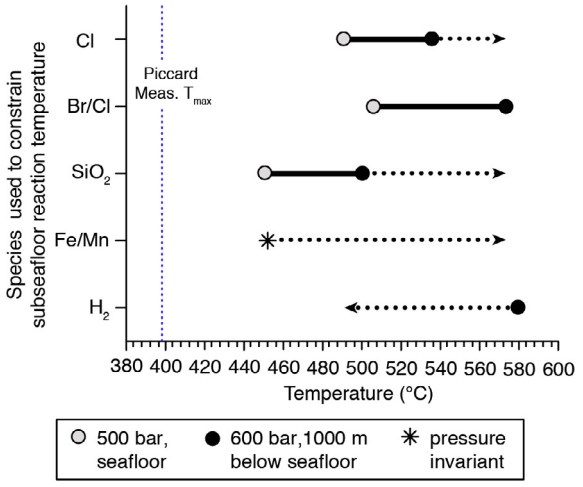

Fig. 13. Summary of subseafloor reaction temperature ranges inferred from various chemical species, compared with measured maximum seafloor fluid temperature at the Beebe Vents (blue dotted line). Temperature constraints are shown for seafloor pressure (500 bar, open circle) and for pressures corresponding to 1000 m deep circulation below seafloor (600 bar, filled circle) for Cl, Br/Cl ratio and SiO_2. For Cl and SiO_2, dotted arrows indicate the possibility of higher temperatures if pressures during deep circulation exceed 600 bar. H_2 abundances that are at equilibration with a HM mineral assemblage in the subsurface at 600 bar bracket the high end of potential subseafloor reaction temperatures, although lower temperatures are also possible. Fe/Mn ratio provides a minimum reaction temperature estimate and is pressure invariant (star). (For interpretation of the references to colour in this figure legend, the reader is referred to the web version of this article.)

fluid. This result argues against a deep abiotic origin for C_{2+} hydrocarbons for the Piccard high temperature vents, and suggests that near-seafloor thermal alteration of biomass may be an important contributor to C_{2+} alkanes in black smokers. Vent chimney morphology may be an important control; i.e., more porous structures may create more low-temperature environments that host microbial biomass in close proximity to high temperature fluid flow, allowing for their interaction.

6. SUMMARY

Vent fluids circulating at Piccard are subject to exceptionally high pressures, relative to all other oceanic ridge-crest hydrothermal systems, due to their setting on the world's deepest mid-ocean ridge crest, the Mid-Cayman Rise. Although the measured maximum temperature of 398 °C is below the two-phase boundary of seawater at seafloor conditions, several lines of evidence suggest that these fluids have cooled from much higher temperatures of fluid/rock reaction at depth. Depletions in Cl in high temperature fluids at Piccard are attributed to phase separation, and require minimum temperatures of 491 °C for phase separation at the seafloor, while phase separation 1000 m below seafloor would have resulted in fluid temperatures exceeding 500 °C (Fig. 13). The high temperature Beebe Vents and Beebe Woods fluids share a common major ion and dissolved volatile chemistry, which reflects a single source fluid that originates at depth in the oceanic lithosphere and feeds the entire Piccard field. Major elements, volatiles, and elemental ratios, including elevated Br/Cl ratios, high SiO_2, ΣH_2S and K contents, and low Ca and Ca/Cl ratios support similarly high temperatures of reaction during formation of Piccard vent fluids. High Cu contents, low Fe/Cu and Mn/Cl ratios, and a high Fe/Mn ratio are also consistent with a high temperature origin for the Piccard fluids. Water/rock ratios of 2, 5 to 16, and 50 to 60 were calculated from dissolved Li, Rb, and Sr abundances and Sr isotopes, respectively.

A striking feature of vent fluid chemistry at Piccard is the very high aqueous H_2 content. The endmember concentration of 19.9 mmol/L at the mafic-hosted Beebe Vents and Beebe Woods is higher than abundances observed at many ultramafic-influenced systems and may be attributed to the exceptionally high temperatures of fluid/rock reaction. These high H_2 concentrations are consistent with redox-dependent fluid-mineral equilibria at temperatures in the vicinity of 500 °C. In addition, H_2 may be generated by the precipitation of pyrite as the fluids cool during ascent. Dissolved ΣCO_2 at Piccard is likely of magmatic origin, as is dissolved He. The origin of CH_4 is equivocal, but may derive from a combination of thermogenic sources and leaching of abiotic CH_4 from mineral-hosted fluid inclusions. Dissolved CO abundances are at equilibrium with the water-gas shift reaction at measured conditions. Elevated dissolved ΣHCOOH in Beebe Woods is consistent with metastable thermodynamic equilibrium for production via ΣCO_2 reduction with H_2 and provides support for an abiotic origin of ΣHCOOH at Piccard. Thermodynamic equilibrium of the ΣCO_2-ΣHCOOH system is delicately poised at Piccard, as ΣHCOOH does not form in measureable quantities at Beebe Vents due to higher temperatures, despite equal compositions of all other relevant species. Small quantities of C_{2+} hydrocarbons (C_2H_6, C_3H_8, n-C_4H_{10}, i-C_4H_{10}) identified in Beebe Vents and Beebe Woods may be derived from an abiotic mantle source, or, more likely, thermal alteration of DOC and POC. These findings expand the known compositional range of high temperature fluid geochemistry in mafic-hosted deep-sea hydrothermal systems.

ACKNOWLEDGEMENTS

This work was supported by the National Aeronautics and Space Administration (NASA) Astrobiology Science and Technology for Exploring Planets program [award number NNX09AB75G to CRG and JSS]; and the National Science Foundation [award number OCE-1061863 to CRG and JSS]. Ship and vehicle time for cruise FK008 was provided by the Schmidt Ocean Institute. We are grateful for invaluable support from the captain and crew of R/V *Atlantis* and R/V *Falkor* and the ROV *Jason II* and HROV *Nereus* technical groups, who provided critical assistance during cruise planning, at sea operations, and vent fluid sample collection. We also wish to thank James Kinsey for providing bathymetric maps, and Meg Tivey, Frieder Klein, and Scott Wankel for sharing thoughtful comments during data analysis and interpretation. This manuscript was improved by constructive reviews from Dionysius Foustoukos and Mike Mottl.

APPENDIX A. SUPPLEMENTARY MATERIAL

Supplementary data associated with this article can be found, in the online version, at https://doi.org/10.1016/j.gca.2018.01.021.

REFERENCES

Albarède F., Michard A., Minster J. F. and Michard G. (1981) $^{86}Sr/^{87}Sr$ ratios in hydrothermal waters and deposits from the East Pacific Rise at 21°N. *Earth and Planet. Sci. Lett.* **55**, 229–236.

Alt J.C. (1995) Subseafloor processes in mid-ocean ridge hydrothermal systems. In: Seafloor Hydrothermal Systems: Physical, Chemical, Biological, and Geological Interactions vol. 91 (eds. S. E. Humphris, R. A. Zierenberg, L. S. Mullineaux and R. E. Thompson) AGU Monograph. American Geophysical Union, pp. 85–114.

Baross J. A. and Deming J. W. (1995) Growth at high temperatures: Isolation and taxonomy, physiology, and ecology. In *The Microbiology of Deep-Sea Hydrothermal Vents* (ed. D. M. Karl). CRC Press, Boca Raton, FL, pp. 169–217.

Beaulieu S. E., Baker E. T., German C. R. and Maffei A. (2013) An authoritative global database for active submarine hydrothermal vent fields. *Geochem. Geophys. Geosys.* **14**, 4892–4905.

Berndt M. E., Seyfried, Jr., W. E. and Beck J. W. (1988) Hydrothermal alteration processes at midocean ridges: experimental and theoretical constraints from Ca and Sr exchange reactions and sr isotopic ratios. *J. Geophys. Res.* **93**, 4573–4583.

Berndt M. E., Seyfried, Jr., W. E. and Janecky D. R. (1989) Plagioclase and epidote buffering of cation ratios in mid-ocean ridge hydrothermal fluids: experimental results in and near the supercritical region. *Geochim. Cosmochim. Acta* **53**, 2283–2300.

Berndt M. E. and Seyfried, Jr., W. E. (1990) Boron, bromine, and other trace elements as clues to the fate of chlorine in mid-ocean ridge vent fluids. *Geochim. Cosmochim. Acta* **54**(8), 2235–2245.

Berndt M. E. and Seyfried, Jr., W. E. (1997) Calibration of Br/Cl fractionation during sub-critical phase separation of seawater: possible halite at 9 to 10°N East Pacific Rise. *Geochim. Cosmochim. Acta* **61**, 2849–2854.

Bischoff J. L. (1991) Densities of liquids and vapors in boiling NaCl-H_2O Solutions – a Pvtx summary from 300 °C to 500 °C. *Am. J. Sci.* **291**, 309–338.

Bischoff J. L. and Dickson F. (1975) Seawater-basalt interaction at 200 °C and 500 bars: implications for origin of sea-floor heavy-metal deposits and regulation of seawater chemistry. *Earth Planet. Sci. Lett.* **25**, 385–397.

Bischoff J. L. and Rosenbauer R. J. (1985) An empirical equation of state for hydrothermal seawater (3.2 percent NaCl). *Am. J. Sci.* **285**, 725–763.

Bischoff J. L. and Rosenbauer R. J. (1988) Liquid-vapor relations in the critical region of the system NaCl-H_2O from 380 to 415 °C: a refined determination of the critical point and two-phase boundary of seawater. *Geochim. Cosmochim. Acta* **52**, 2121–2126.

Bischoff J. L. and Pitzer K. S. (1989) Liquid-vapor relations for the system NaCl-H_2O: summary of the PTX surface from 300° to 500 °C. *Am. J. Sci.* **289**, 217–248.

Bowers T. S., Von Damm K. L. and Edmond J. M. (1985) Chemical evolution of mid-ocean ridge hot springs. *Geochim. Cosmochim. Acta* **49**, 2239–2252.

Brimhall G. H. and Crerar D. A. (1987) Ore fluids: magmatic to supergene. In Thermodynamic Modeling of Geological Materials: Minerals, Fluids and Melts (eds I. S. E. Carmichael and H. P. Eugster). Rev. in Mineral. vol 17, Min Soc. Am. pp. 235–321.

Butterfield D. A., Roe K. K., Lilley M. D., Huber J. A., Baross J. A., Embley R. W. and Massoth G. J. (2004) Mixing, reaction and microbial activity in the sub-seafloor revealed by temporal and spatial variation in diffuse flow vents at axial volcano. In The Subseafloor Biosphere at Mid-Ocean Ridges (eds. W. S. D. Wilcock, E. F. Delong, D. S. Kelley, J. A. Baross and S. C. Cary), American Geophysical Union Geophys. Mono. Ser., vol. 144, Washington, D.C. pp. 269–289.

Butterfield D. A. and Massoth G. J. (1994) Geochemistry of North Cleft segment vent fluids: temporal changes in chlorinity and their possible relation to recent volcanism. *J. Geophys. Res.* **99** (B3), 4951–4968.

Butterfield D. A., Jonasson I. R., Massoth G. J., Feely R. A., Roe K. K., Embley R. E., Holden J. F., McDuff R. E., Lilley M. D. and Delaney J. R. (1997) Seafloor eruptions and evolution of hydrothermal fluid chemistry. *Philos. Trans. Roy. Soc. Lond. A* **355**, 369–386.

Charlou J. L., Donval J. P., Jean-Baptiste P., Dapoigny A. and Rona P. A. (1996) Gases and helium isotopes in high temperature solutions sampled before and after ODP 158 drilling at TAG hydrothermal field (26°N, MAR). *Geophys. Res. Lett.* **23**, 3491–3494.

Charlou J. L., Donval J. P., Fouquet Y., Jean-Baptiste P. and Holm N. (2002) Geochemistry of high H_2 and CH_4 vent fluids issuing from ultramafic rocks at the Rainbow hydrothermal field (36°14′N, MAR). *Chem. Geol.* **191**, 345–359.

Charlou J. L., Donval J. P., Konn C., Ondreacuteas H., Fouquet Y., Jean-Baptiste P. and Fourr E. (2010) High production and fluxes of H2 and CH4 and evidence of abiotic hydrocarbon synthesis by serpentinization in ultramafic-hosted hydrothermal systems on the Mid-Atlantic Ridge. In Diversity of Hydrothermal Systems on Slow Spreading Ocean Ridges, vol. 188 (eds. P. A. Rona, C. W. Devey, J. Dyment and B. J. Murton) AGU Monograph. American Geophysical Union, pp. 265–296.

Cohen R. S. and O'Nions R. K. (1982) The lead, neodymium and strontium isotopic structure of ocean ridge basalts. *J. Petrol.* **23**, 299–324.

Connelly D. P., Copley J. T., Murton B. J., Stansfield K., Tyler P. A., German C. R., Van Dover C. L., Amon D., Furlong M., Grindlay N., Hayman N., Hühnerbach V., Judge M., Le Bas T., McPhail S., Meier A., Nakamura K., Nye V., Pebody M., Pedersen R. B., Plouviez S., Sands C., Searle R. C., Stevenson P., Taws S. and Wilcox S. (2012) Hydrothermal vent fields and chemosynthetic biota on the world's deepest seafloor spreading centre. *Nat. Commun.* **2**, 1–9.

Craddock P. R. (2009) Geochemical Tracers of Processes Affecting the Formation of Seafloor Hydrothermal Fluids and Deposits in the Manus Back-arc Basin. Ph.D. thesis, MIT-WHOI Joint Program in Oceanography, MIT.

Craig H. and Lupton J. E. (1976) Primordial neon, helium, and hydrogen in oceanic basalts. *Earth Planet. Sci. Lett.* **31**, 369–385.

Cruse A. and Seewald J. S. (2006) Geochemistry of low-molecular weight hydrocarbons in hydrothermal fluids from Middle Valley, northern Juan de Fuca Ridge. *Geochim. Cosmochim. Acta* **70**, 2073–2092.

Dick G. J., Anantharaman K., Baker B. J., Li M., Reed D. C. and Sheik C. S. (2013) The microbiology of deep-sea hydrothermal vent plumes: ecological and biogeographical linkages to seafloor and water column habitats. *Front. Microbiol.* **4**(124). https://doi.org/10.3389/fmicb.2013.00124.

Douville E., Charlou J. L., Oelkers E., Bienvenu P., Colon C., Donval J., Fouquet Y., Prieur D. and Appriou P. (2002) The Rainbow vent fluids (36°14′N, MAR): the influence of ultramafic rocks and phase separation on trace metal content in Mid-Atlantic Ridge hydrothermal fluids. *Chem. Geol.* **184**, 37–48.

Driesner T. and Heinrich C. (2007) The system H_2O-NaCl. Part I: Correlation formulae for phase relations in temperature-pressure-composition space from 0 to 1000 °C, 0 to 5000 bar, and 0 to $1x_{NaCl}$. *Geochim. Cosmochim. Acta* **71**, 4880–4901.

Druffel E. R. M., Williams P. M., Bauer J. E. and Ertel J. R. (1992) Cycling of dissolved and particulate organic matter in the open ocean. *J. Geophys. Res.: Oceans* **97**(C1), 15639–15659.

Elthon D., Ross D. K. and Meen J. K. (1995) Compositional variations of basaltic glasses from the Mid-Cayman Rise spreading center. *J. Geophys. Res: Solid Earth* **1978–2012** (100), 12497–12512.

Evans W. C., White L. D. and Rapp J. B. (1988) Geochemistry of some gases in hydrothermal fluids from the southern Juan de Fuca Ridge. *J. Geophys. Res.* **93**, 15305–15313.

Fernández D. P., Goodwin A. R. H., Lemmon E. W., Levelt Sengers J. M. H. and Williams R. C. (1997) A formulation for the static permittivity of water and steam at temperatures from 238 K to 873 K at pressures up to 1200 MPa, including derivatives and debye-hückel coefficients. *J. Phys. Chem. Ref. Data* **26**, 1125.

Fontaine F. J., Wilcock W. S. D., Foustoukos D. E. and Butterfield D. A. (2009) A Si-Cl geothermobarometer for the reaction zone of high-temperature, basaltic-hosted mid-ocean ridge hydrothermal systems. *Geochem. Geophys. Geosyst.* **10**.

Foustoukos D. I. and Seyfried, Jr., W. E. (2004) Hydrocarbons in hydrothermal vent fluids: the role of chromium-bearing catalysts. *Science* **304**(5673), 1002–1005.

Foustoukos D. I. and Seyfried, Jr., W. E. (2005) Redox and pH constraints in the subseafloor root zone of the TAG hydrothermal system, 26°N Mid-Atlantic Ridge. *Earth Planet. Sci. Lett.* **235**, 497–510.

Foustoukos D. I. and Seyfried, Jr., W. E. (2007a) Trace element partitioning between vapor, brine and halite under extreme phase separation conditions. *Geochim. Cosmochim. Acta* **71**, 2056–2071.

Foustoukos D. I. and Seyfried, Jr., W. E. (2007b) Fluid phase separation processes in submarine hydrothermal systems. *Rev. Mineral. Geochem.* **65**, 213–239.

Foustoukos D. I., Pester N. J., Ding K. and Seyfried, Jr., W. E. (2009) Dissolved carbon species in associated diffuse and focused flow hydrothermal vents at the Main Endeavour Field, Juan de Fuca Ridge: Phase equilibria and kinetic constraints. *Geochem. Geophys. Geosyst.* **10**. https://doi.org/10.1029/2009GC002472.

Gallant R. M. and Von Damm K. L. (2006) Geochemical controls on hydrothermal fluids from the Kairei and Edmond Vent Fields, 23°–25°S, Central Indian Ridge. *Geochem. Geophys. Geosys.* **7**. https://doi.org/10.1029/2005GC001067.

Gao X. and Thiemens M. H. (1991) Systematic study of sulfur isotopic composition in iron meteorites and the occurrence of excess ^{33}S and ^{36}S. *Geochim. Cosmochim. Acta* **55**, 2671–2679.

German C. R., Bowen A., Coleman M., Honig D., Huber J., Jakuba M., Kinsey J., Kurz M., Leroy S., McDermott J. M., Mercier de Lépinay B., Nakamura K., Seewald J. S., Smith J. L., Sylva S. P., Van Dover C. L., Whitcomb L. L. and Yoerger D. R. (2010) Diverse styles of submarine venting on the ultraslow spreading Mid-Cayman Rise. *Proc. Nat. Acad. Sci.* **107**, 14020.

German C. R. and Seyfried, Jr, W. E. (2014) Hydrothermal Processes. In *Treatise on Geochemistry* (eds. H. D. Holland and K. K. Turekian), Second Edition. Elsevier, Oxford, pp. 191–233.

Hall O. and Aller R. (1992) Rapid, small-volume, flow injection analysis for ΣCO2 and NH4+ in marine and freshwaters. *Limnol. Oceanogr.* **37**, 1113–1119.

Hansell D. A. and Carlson C. A. (1998) Deep-ocean gradients in the concentration of dissolved organic carbon. *Nature* **395**, 263–266.

Hayman N. W., Grindlay N. R., Perfit M. R., Mann P., Leroy S. and de Lépinay B. M. (2011) Oceanic core complex development at the ultraslow spreading Mid-Cayman Spreading Center. *Geochem. Geophys. Geosys.* **12**. https://doi.org/10.1029/2010GC003240.

Helgeson H. C. (1992) Effects of complex formation in flowing fluids on the hydrothermal solubilities of minerals as a function of fluid pressure and temperature in the critical and supercritical regions of the system H_2O. *Geochim. Cosmochim. Acta* **56**, 3191–3207.

Horita J. (2001) Carbon isotope exchange in the system CO_2-CH_4 at elevated temperatures. *Geochim. Cosmochim. Acta* **65**, 1907–1919.

Huber J. A., Welch D. B. M., Morrison H. G., Huse S. M., Neal P. R., Butterfield D. A. and Sogin M. L. (2007) Microbial population structures in the deep marine biosphere. *Science (80)* **318**, 97–101.

Jackson M. G. and Hart S. R. (2006) Strontium isotopes in melt inclusions from Samoan basalts: Implications for heterogeneity in the Samoan plume. *Earth Planet. Sci. Lett.* **245**, 260–277.

Johnson J., Oelkers E. and Helgesen H. (1992) SUPCRT92: a software package for calculating the standard molal thermodynamic properties of minerals, gases, aqueous species, and reactions from 1 to 5000 bar and 0 to 1000 °C. *Comput. Geosci.* **18**, 899–947.

Kelley D. S., Baross J. A. and Delaney J. R. (2002) Volcanoes, fluids, and life at mid-ocean ridge spreading centers. *Annu. Rev. Earth Planet. Sci.* **30**, 385–491.

Kadko D. and Butterfield D. A. (1998) The relationship of hydrothermal fluid composition and crustal residence time to maturity of vent fields on the Juan de Fuca Ridge. *Geochim. Cosmochim. Acta* **62**, 1521–1533.

Kelley D. S. and Früh-Green G. L. (1999) Abiogenic methane in deep-seated mid-ocean ridge environments: Insights from stable isotope analyses. *J. Geophys. Res.* **104**, 10439–10460.

Kinsey J. C. and German C. R. (2013) Sustained volcanically-hosted venting at ultraslow ridges: Piccard Hydrothermal Field, Mid-Cayman Rise Earth Planet. *Sci. Lett.* **380**, 162–168.

Klein E. M. and Langmuir C. H. (1987) Global correlations of ocean ridge basalt chemistry with axial depth and crustal thickness. *J. Geophys. Res.: Solid Earth* **92**, 8089–8115.

Koschinsky A., Garbe-Schönberg D., Sander S., Schmidt K., Gennerich H. H. and Strauss H. (2008) Hydrothermal venting at pressure-temperature conditions above the critical point of seawater, 5°S on the Mid-Atlantic Ridge. *Geology* **36**, 615.

Lilley M. D., Butterfield D. A., Lupton J. E. and Olson E. J. (2003) Magmatic events can produce rapid changes in hydrothermal vent chemistry. *Nature* **422**, 878–881.

Lott D. E. (2001) Improvements in noble gas separation methodology: A nude cryogenic trap. *Geochem. Geophys. Geosys.* **1**(12). https://doi.org/10.1029/2001GC000202.

Lupton J. E. and Craig H. (1975) Excess ^3He in oceanic basalts: evidence for terrestrial primordial helium. *Earth Planet. Sci. Lett.* **26**, 133–139.

Macleod G., McKeon C., Hall A. J. and Russell M. J. (1994) Hydrothermal and oceanic pH conditions of possible relevance to the origin of life. *Orig. Life Evol. Biosph.* **24**(1), 19–41.

Martin W., Baross J., Kelley D. and Russell M. J. (2008) Hydrothermal vents and the origin of life. *Nature Rev. Microbiol.* **6**, 805–814.

Marty B. and Tolstikhin I. N. (1998) CO_2 fluxes from mid-ocean ridges, arcs and plumes. *Chem. Geol.* **145**, 233–248.

McCollom T. M. and Seewald J. S. (2007) Abiotic synthesis of organic compounds in deep-sea hydrothermal environments. *Chem. Rev.* **107**, 382–401.

McCollom M. and Shock E. L. (1998) Fluid-rock interactions in the lower oceanic crust : Thermodynamic models of hydrothermal alteration Rocks from the lower oceanic crust show both petrologic and isotopic evidence for extensive alteration by circulating hydrothermal fluids derived from Dee. *J. Geophys. Res.* **103**, 545–575.

McDermott J. M., Ono S., Tivey M. K., Seewald J. S., Shanks, III, W. C. and Solow A. R. (2015a) Identitfication of sulfur sources and isotopic equilibria in submarine hot-springs using multiple sulfur isotopes. *Geochim. Cosmochim. Acta* **160**, 169–187.

McDermott J. M., Seewald J. S., German C. R. and Sylva S. P. (2015b) Pathways for abiotic organic synthesis at submarine hydrothermal fields. *Proc. Nat. Acad. Sci.* **112**, 7668–7672.

Merlivat L., Pineau F. and Javoy M. (1987) Hydrothermal vent waters at 13°N on the East Pacific Rise: isotopic composition and gas concentration. *Earth Planet Sci. Lett.* **84**, 100–108.

Mottl M. J., Holland H. D. and Corr R. F. (1979) Chemical exchange during hydrothermal alteration of basalt by seawater – II. Experimental results for Fe, Mn and sulfur species. *Geochim. Cosmochim. Acta* **43**, 869–884.

Mottl M. J. and Holland H. D. (1978) Chemical exchange during hydrothermal alteration of basalt by seawater – I. Experimental results for major and minor components of seawater. *Geochim. Cosmochim. Acta* **42**, 1103–1115.

Oelkers and Helgeson (1990) Triple-ion anions and polynuclear complexing in supercritical electrolyte solutions. *Geochim. Cosmochim. Acta* **54**(3), 727–738.

Olsson I. (1970) The use of oxalic acid as a standard. In Radiocarbon Variations and Absolute Chronology. Nobel Symposium 12th Proc. (ed. Olsson I.) John Wiley & Sons, New York, p. 17.

Ono S., Wing B., Rumble D. and Farquhar J. (2006) High precision analysis of all four stable isotopes of sulfur (32S, 33S,

34S and 36S) at nanomole levels using a laser fluorination isotope-ratio-monitoring gas chromatography–mass spectrometry. *Chem. Geol.* **225**, 30–39.

Oremland R. S. and Des Marais D. J. (1983) Distribution, abundance and carbon isotopic composition of gaseous hydrocarbons in Big Soda Lake, Nevada: an alkaline, meromictic lake. *Geochim. Cosmochim. Acta* **47**, 2107–2114.

Pester N. J., Rough M., Ding K. and Seyfried, Jr., W. E. (2011) A new Fe/Mn geothermometer for hydrothermal systems: Implications for high-salinity fluids at 13°N on the East Pacific Rise. *Geochim. Cosmochim. Acta* **75**, 7881–7892.

Pester N. J., Ding K. and Seyfried, Jr., W. E. (2014) Magmatic eruptions and iron volatility in deep-sea hydrothermal fluids. *Geology* **42**, 255–258.

Perfit M. R. and Heezen B. C. (1978) The geology and evolution of the Cayman Trench. *Geol. Soc. Am. Bull.* **89**, 1155–1174.

Pindell J. L. and Barrett S. F. (1990) Geological evolution of the Caribbean region; A plate-tectonic perspective. In The Caribbean Region: The Geology of North America (eds. Dengo G. and Case J. E.) The Geological Society of America, vol. H, Boulder, Colorado. p. 405–432.

Pineau F. and Javoy M. (1983) Carbon isotopes and concentrations in mid-oceanic ridge basalts. *Earth Planet. Sci. Lett.* **62**, 239–257.

Proskurowski G., Lilley M. D. and Olson E. J. (2008) Stable isotopic evidence in support of active microbial methane cycling in low-temperature diffuse flow vents at 9°50′N East Pacific Rise. *Geochim. Cosmochim. Acta* **72**, 2005–2023.

Ravizza G., Blusztajn J., Von Damm K. L., Bray A., Bach W. and Hart S. (2001) Sr isotope variations in vent fluids from 9°46′–9°54′N East Pacific Rise: evidence of a non-zero-Mg fluid component. *Geochim. Cosmochim. Acta* **65**, 729–739.

Rees C., Jenkins W. and Monster J. (1978) The sulphur isotopic composition of ocean water sulphate. *Geochim. Cosmochim. Acta* **42**, 377–381.

Reeves E. P., Seewald J. S., Saccocia P., Bach W., Craddock P. R., Shanks, III, W. C., Sylva S. P., Walsh E., Pichler T. and Rosner M. (2011) Geochemistry of hydrothermal fluids from the PACMANUS, Northeast Pual and Vienna Woods hydrothermal fields, Manus Basin, Papua New Guinea. *Geochim. Cosmochim. Acta* **75**, 1088–1123.

Reeves E. P., McDermott J. M. and Seewald J. S. (2014) Methanethiol production in mid-ocean ridge hydrothermal fluids. *Proc. Nat. Acad. Sci.* **111**(15), 5474–5479.

Rosencrantz E., Ross M. and Sclater J. (1988) Age and spreading history of the cayman trough as determined from depth, heat-flow, and magnetic-anomalies. *J. Geophys. Res: Solid Earth Planets* **93**, 2141–2157.

Russell M. J., Hall A. J. and Martin W. (2010) Serpentinization as a source of energy at the origin of life. *Geobiology* **8**, 355–371.

Sakai H., Des Marais D. J., Ueda A. and Moore J. G. (1984) Concentrations and isotope ratios of carbon, nitrogen and sulfur in ocean-floor basalts. *Geochim. Cosmochim. Acta* **48**, 2433–2441.

Seyfried, Jr, W. E., Ding K. and Berndt M. E. (1991) Phase equilibria constraints on the chemistry of hot spring fluids at mid-ocean ridges. *Geochim. Cosmochim. Acta* **55**, 3559–3580.

Seewald J. S. and Seyfried, Jr., W. E. (1990) The effect of temperature on metal mobility in subseafloor hydrothermal systems: constraints from basalt alteration experiments. *Earth Planet. Sci. Lett.* **101**, 388–403.

Seewald J. S., Doherty K. W., Hammar T. R. and Liberatore S. P. (2002) A new gas-tight isobaric sampler for hydrothermal fluids. *Deep Sea Res. I: Oceanographic Res. Papers* **49**, 189–196.

Seewald J. S., Cruse A. and Saccocia P. (2003) Aqueous volatiles in hydrothermal fluids from the Main Endeavour Field, northern Juan de Fuca Ridge: temporal variability following earthquake activity. *Earth Planet. Sci. Lett.* **216**, 575–590.

Seewald J. S., Zolotov M. Y. and McCollom T. (2006) Experimental investigation of single carbon compounds under hydrothermal conditions. *Geochim. Cosmochim. Acta* **70**(2), 446–460.

Seyfried, Jr., W. E. and Bischoff J. (1981) Experimental seawater-basalt interaction at 300 °C, 500 bars, chemical exchange, secondary mineral formation and implications for the transport of heavy metals. *Geochim. Cosmochim. Acta* **45**, 135–147.

Seyfried, Jr., W. E., Janecky D. R. and Mottl M. J. (1984) Alteration of the oceanic crust: implications for geochemical cycles of lithium and boron. *Geochim. Cosmochim. Acta* **48**, 557–569.

Seyfried, Jr., W. E. and Janecky D. R. (1985) Heavy metal and sulfur transport during subcritical and supercritical hydrothermal alteration of basalt: influence of fluid pressure and basalt composition and crystallinity. *Geochim. Cosmochim. Acta* **49**, 2545–2560.

Seyfried, Jr., W. E. (1987) Experimental and theoretical constraints on hydrothermal alteration processes at mid-ocean ridges. *Ann. Rev. Earth Planet. Sci.* **15**, 317–335.

Seyfried W. E. and Ding K. (1993) The effect of redox on the relative solubilities of copper and iron in Cl-bearing aqueous fluids at elevated temperatures and pressures: an experimental study with application to subseafloor hydrothermal systems. *Geochim. Cosmochim. Acta* **57**, 1905–1917.

Seyfried Jr., W. E. and Ding K. (1995) Phase equilibria in subseafloor hydrothermal systems: a review of the role of redox, temperature, pH and dissolved Cl on the Chemistry of Hot Spring Fluids at Mid-Ocean Ridges. In Seafloor Hydrothermal Systems: Physical, Chemical, Biological, and Geological Interactions vol. 91 (eds. S. E. Humphris, R. A. Zierenberg, L. S. Mullineaux and R. E. Thompson) AGU Monograph. American Geophysical Union, pp. 248–272.

Seyfried, Jr., W. E., Seewald J. S., Berndt M. E., Ding K. and Foustoukos D. I. (2003) Chemistry of hydrothermal vent fluids from the Main Endeavour Field, Northern Juan de Fuca Ridge: geochemical controls in the aftermath of June 1999 seismic events. *J. Geophys. Res.* **108**(2429), 2410.1029/ 2002JB001957.

Seyfried Jr., W. E., Foustoukos D. I. and Allen D. E. (2004) Ultramafic-Hosted Hydrothermal Systems at Mid-Ocean Ridges: Chemical and Physical Controls on pH, Redox and Carbon Reduction Reactions. In Mid-Ocean Ridges American Geophysical Union. pp. 267–284.

Shanks, III, W. C. (2001) Stable isotopes in seafloor hydrothermal systems: vent fluids, hydrothermal deposits, hydrothermal alteration, and microbial processes. *Rev. Min. Geochem.* **43**, 469–525.

Shanks, III, W. C. and Seyfried, Jr., W. E. (1987) Stable isotope studies of vent fluids and chimney minerals, southern Juan de Fuca Ridge: Sodium metasomatism and seawater sulfate reduction. *J. Geophys. Res. Solid Earth* **92**, 11387–11399.

Shock E. L., Helgeson H. C. and Sverjensky D. A. (1989) Calculation of the thermodynamic and transport properties of aqueous species at high pressures and temperatures: standard partial molal properties of inorganic neutral species. *Geochim. Cosmochim. Acta* **53**, 2157–2183.

Shock E. L. (1990) Geochemical constraints on the origin of organic compounds in hydrothermal systems. *Orig. life Evol. Biosph.* **20**, 331–367.

Shock E. L. (1992) Chemical environments of submarine hydrothermal systems. *Orig. Life Evol. Biosph.* **22**, 67–107.

Shock E. L. and Helgeson H. C. (1990) Calculation of the thermodynamic and transport properties of aqueous species at high pressures and temperatures: standard partial molal prop-

erties of organic species. *Geochim. Cosmochim. Acta* **54**, 915–945.

Stoessel R. K. and Carpenter A. D. (1986) Stoichiometric saturation tests of $NaCl_{1-X}Br_X$ and $KCl_{1-X}Br_X$. *Geochim. Cosmochim. Acta* **50**, 1465–1474.

Stoessel R. K. (1992) Comment on "Reaction paths and equilibrium end-points in solid-solution systems" by P.J. Glynn, E.J. Reardon, L.N. Plummer and E. Busenberg. *Geochim. Cosmochim. Acta* **56**, 2555–2557.

ten Brink U., Coleman D. and Dillon W. (2002) The nature of the crust under Cayman Trough from gravity. *Mar. Petrol. Geol.* **19**, 971–987.

Tolstikhin I. N. and Marty B. (1998) The evolution of terrestrial volatiles: a view from helium, neon, argon and nitrogen isotope modelling. *Chem Geol.* **147**, 27–52.

Von Damm K. L., Edmond J. M., Grant B., Walden B. and Weiss R. F. (1985) Chemistry of submarine hydrothermal solutions at 21°N, East Pacific Rise. *Geochim. Cosmochim. Acta* **49**, 2197–2220.

Von Damm K. L. (1990) Seafloor hydrothermal activity: black smoker chemistry and chimneys. *Ann. Rev. Earth Planet. Sci.* **18**, 173.

Von Damm K. L., Bischoff J. and Rosenbauer R. (1991) Quartz solubility in hydrothermal seawater: an experimental study and equation describing quartz solubility for up to 0.5 M NaCl solutions. *Am. J. Sci.* **291**, 977–1007.

Von Damm K. L. (1995) Controls on the chemistry and temporal variability of seafloor hydrothermal fluids. In Seafloor Hydrothermal Systems: Physical, Chemical, Biological, and Geological Interactions vol. 91 (eds. S. E. Humphris, R. A. Zierenberg, L. S. Mullineaux and R. E. Thompson) AGU Monograph. American Geophysical Union, Washington DC, pp. 222–247.

Von Damm K. L. (2000) Chemistry of hydrothermal vent fluids from 9–10°N, East Pacific Rise: "Time zero", the immediate posteruptive period. *J. Geophys. Res: Solid Earth* **105**, 11203–11222.

Von Damm K. L. and Lilley M. D. (2004) Diffuse flow hydrothermal fluids from 9°50′N East Pacific Rise: Origin, evolution and biogeochemical controls. In The Subseafloor Biosphere at Mid-Ocean Ridges vol. 144 (eds. W. S. D. Wilcock, E. F. DeLong, D. S. Kelley, J. A. Baross, S. C. Cary) AGU Monograph. American Geophysical Union, Washington DC, pp. 245–268.

Voss B. M., Peucker-Ehrenbrink B., Eglinton T. I., Fiske G., Wang Z. A., Hoering K. A., Montluçon D. B., LeCroy C., Pal S., Marsh S., Gillies S. L., Janmaat A., Bennett M., Downey B., Fanslau J., Fraser H., Macklam-Harron G., Martinec M. and Wiebe B. (2014) Tracing river chemistry in space and time: dissolved inorganic constituents of the Fraser River, Canada. *Geochim. Cosmochim. Acta* **124**, 283–308.

Webber A. P., Roberts S., Murton B. J. and Hodgkinson M. R. S. (2015) Geology, sulfide geochemistry and supercritical venting at the Beebe Hydrothermal Vent Field, Cayman Trough. *Geochem. Geophys. Geosys.* **16**, 2661–2678. https://doi.org/10.1002/2015GC005879.

Welhan J. A. and Craig H. (1983) Methane, Hydrogen and Helium in Hydrothermal Fluids at 21°N on the East Pacific Rise. In Hydrothermal Processes at Seafloor Spreading Centers (eds. Rona P. A., Boström K., Laubier L., Smith Jr., K. L.) NATO Conference Series vol. 12, Springer U.S., pp. 391–409.

Welhan J. A. (1988) Origins of methane in hydrothermal systems. *Chem. Geol.* **71**, 183–198.

Wilson S. C., Murton B. J. and Taylor R. N. (2013) Mantle composition controls the development of an Oceanic Core Complex. *Geochem. Geophys. Geosys* **14**(4), 1–18. https://doi.org/10.1002/ggge.20046.

Woodruff L. G. and Shanks W. C. (1988) Sulfur isotope study of chimney minerals and vent fluids from 21°N, East Pacific Rise: Hydrothermal sulfur sources and disequilibrium sulfate reduction. *J. Geophys. Res.* **93**, 4562–4572.

Associate Editor: Rachael James